이학석사 학위논문

전고체 리튬전지용 (100-x)Li$_6$PS$_5$Cl-xLiNbO$_3$

(x = 0,2,3,4, and 5) 고체전해질의 향상된

전기화학적 성능과 복합 양극에서의 효과에 관한

연구

Enhanced electrochemical performance of

(100-x)Li$_6$PS$_5$Cl-xLiNbO$_3$ (x = 0, 2, 3, 4, and 5) solid

electrolyte and its effect on composite cathode for all-

solid-state lithium ion batteries

울 산 대 학 교 대 학 원

화 학 과

조 지 운

전고체 리튬전지용 (100-x)Li$_6$PS$_5$Cl-xLiNbO$_3$ (x = 0,2,3,4, and 5) 고체전해질의 향상된 전기화학적 성능과 복합 양극에서의 효과에 관한 연구

Enhanced electrochemical performance of (100-x)Li$_6$PS$_5$Cl-xLiNbO$_3$ (x = 0, 2, 3, 4, and 5) solid electrolyte and its effect on composite cathode for all-solid-state lithium ion batteries

지 도 교 수   류 광 선

이 논문을 이학 석사 학위 논문으로 제출함

2021년 12월

울 산 대 학 교 대 학 원

화 학 과

조지운

조지운의 이학석사 학위 논문을 인준함

위원장   정 재 훈   印

위 원   오 은 석   印

위 원   류 광 선   印

울 산 대 학 교 대 학 원
2021년 12월

감사의 글

Abstract

All-solid-state lithium ion batteries (ASSLBs) are attracting attention as next generation batteries, owing to their high energy density, wide operating temperature and good safety. Among solid electrolytes, especially, sulfide-based solid electrolytes have good elasticity and softness properties and have ionic conductivities comparable to those of conventional organic liquid electrolytes. However, one of the limitations in applying sulfide-based solid electrolyte to ASSLBs is that the interfacial resistance increases during cycling due to its poor electrochemical and mechanical stability.

In this work, we have prepared the $LiNbO_3$ coating material mixed/doped Li_6PS_5Cl solid electrolyte for improving the ionic conductivity and the promoting the interfacial stability between the cathode active material and solid electrolyte.

The different molar ratios of $LiNbO_3$ mixed/doped Li_6PS_5Cl solid electrolyte were prepared by high energy ball mill process and subsequent heat treatment. The powder X-ray diffraction analysis revealed the formation of argyrodite structure. The effect of $LiNbO_3$ addition was confirmed by laser Raman spectroscopy and field emission scanning electron microscopy with EDS analysis. Among the prepared solid electrolytes, $96(Li_6PS_5Cl)$-$4(LiNbO_3)$ solid electrolyte showed high ionic conductivity value of 4.29 mS cm^{-1}, at room temperature. The prepared solid electrolytes exhibited good electrochemical stability against lithium metal. Furthermore, the effect of the addition of $LiNbO_3$ was analyzed by charge–discharge method and electrochemical impedance spectroscopy (EIS). The ASSLB assembled based on the prepared $LiNbO_3$ mixed/doped Li_6PS_5Cl solid electrolyte/NCM811 composite cathode achieved a high specific capacity (188.69 mAh g^{-1}) and improved the C-rate performance compared to the battery with Li_6PS_5Cl solid electrolyte/NCM811 composite cathode (163.41 mAh g^{-1}).

Contents

Chapter 1. Introduction

Chapter 2. General experimental

Chapter 3. Synthesis and electrochemical performance of (100-x)(Li$_6$PS$_5$Cl)-xLiNbO$_3$ solid electrolyte for all-solid-state lithium batteries

Chapter 4. Summary

List of Tables

List of figures

NCM-(SE)/ SE /Li-In ASSLBs at 25℃. (c) Impedance spectra of the NCM-

(SE)/ SE /Li-In ASSLBs before and after cycling.

Figure 3.7. FE-SEM and EDS mapping images of 96LPSCl-4LNO

solid electrolyte/NCM811 composite cathode after charge-discharge cycles.

Chapter 1. Introduction

1-1. Lithium ion secondary batteries

Lithium ion secondary batteries have been steadily being used in various electronic devices such as cell phone, laptop and many portable devices. Moreover, these batteries have been applied to large scale energy devices such as electrical vehicles (EVs), hybrid electrical vehicles (HEVs) and energy storage system (ESS). The first lithium-ion (Li-ion) batteries were introduced by Sony Corporation in 1991, and are still dominating consumer electronics as a reliable means of energy. Among the commercialized secondary batteries, Li-ion batteries have showed the highest energy (250Wh Kg^{-1}), powder density, and long cycle life. However, Li-ion secondary batteries have several problems in safety. In particular, since the organic liquid electrolyte is used, there is a risk of thermal runaway and explosion in case of leakage. For examples, many EVs and smartphones have exploded due to problems with their built-in batteries. To overcome this problem, many researchers have been tried to develop a new material composition and systems.

1-1-1. Composition of lithium ion batteries

Lithium-ion (Li-ion) batteries are basically composed of cathode, anode, separator, and electrolyte. In general, the conventional cathode materials involving intercalation and extraction of lithium ions with 1-D olivine ($LiFePO_4$), 2-D layered ($LiCoO_2$), and 3-D spinel ($LiMn_2O_4$) structures as shown in Figure 1.1. Typically, $LiCoO_2$ have been used due to its working voltage (3.0-4.5V vs. Li/Li^+) and good cycle life (>500 cycles). The properties of various cathode materials used in commercial Li-ion batteries are listed in Table 1.1. Representatively, there are anode materials such as graphite, silicon and lithium metal. Graphite has a low theoretical specific capacity of 372$mAhg^{-1}$. Silicon theoretically has a specific capacity of 4200mAg^{-1}, but it undergoes significant volume changes and mechanical damage during lithiation and delithiation. Li metal is the ideal anode for Li-ion chemistry which has a theoretical specific capacity of 3860$mAhg^{-1}$ and the lowest negative electrochemical potential of -3.040V vs standard hydrogen electrode. Separator that prevents

a short circuit between the cathode and the anode and allows the electrolyte to permeate is mainly composed of a thin film of porous polyethylene and polypropylene. Organic liquid electrolyte materials such as ethylene carbonate-dimethyl carbonate (EC-DMC) including lithium salt (e.g. $LiPF_6$) are used due to its high ionic conductivity and broad stability of voltage window (0-4.5V vs. Li/Li^+).

1-1-2. Principle of lithium ion batteries

The operating principle of Li-ion secondary batteries is shown in Figure 1.2. Secondary batteries mean that the batteries can repeatedly transfer lithium ion between the cathode and anode through charging or discharging. For example, the cathode and anode materials are oxidized and reduced respectively at charging step. The chemical reactions during charging and discharging can be expressed thorough these equations as follows:

Cathode: $\qquad LiCoO_2 \leftrightarrow Li_{1-x}CoO_2 + xLi + xe^-$ (1.1)

Anode: $\qquad C_6 + xLi + xe^- \leftrightarrow Li_xC_6$ (1.2)

Overall: $\qquad LiCoO_2 + C_6 \leftrightarrow Li_{1-x}CoO_2 + Li_xC_6$ (1.3)
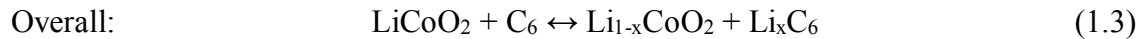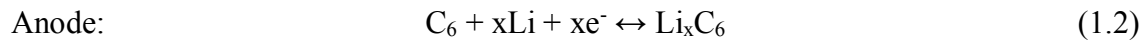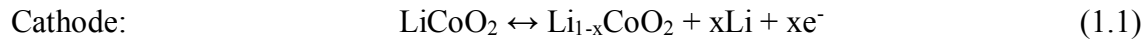
During charging, through the above these chemical reactions, lithium ions are deintercalated from the cathode materials and the released lithium ions are diffused and intercalated to the surface and structure of the anode materials. The electrons move through the external circuit connected to the current collectors. The chemical energy produced by the chemical reaction can be converted and stored to electronic energy according to the Nernst equation:

$$\Delta G = -nFE$$ (1.4)

where G is Gibbs energy, n is number of electrons, F is Faraday`s constant number, and E is electric potential. This equation implies that the electric potential energy is proportional to

the chemical energy, which means that a large chemical potential difference between the cathode and anode leads to a large electric potential and energy. The electric potential proportional to the chemical energy is called to the open circuit voltage (OCV) and is determined within the band gap of the electrolyte, which is determined by the difference in energy between the highest occupied molecular orbital (HOMO) and the lowest unoccupied molecular orbital (LUMO) of the electrolyte as shown in Figure 1.3 [1-3].

1-1-3. Properties and limitation of organic liquid electrolyte

A commercial organic liquid electrolyte is composed of a mixture of two or more kinds of carbonate-based materials and lithium salts such as ethyl carbonate (EC)/dimethyl carbonate (DMC)=1:1 in 1M LiFP$_6$. The electrolytes have been applied to many lithium-based batteries due to its good dielectric constant and electrochemical stability compare to aqueous electrolytes. However, in order to apply to large scale energy devices, the electrolytes must meet the following several requirements: [4]

1)   Retention of the SEI during charge and discharge

2)   A Li+ ion conductivity $\sigma_{Li} > 10^{-4} S/cm$

3)   An electronic conductivity $\sigma_e < 10^{-10} S/cm$

4)   A transference number $\sigma_{Li}/\sigma_{total} \approx 1$, where σ_{total} includes conductivities by other ions in the electrolyte

5)   Chemical stability over wide temperature ranges

Among them, there are conditions in which the organic liquid electrolyte does not satisfy a low transference number, chemical stability, electrochemical stability, and the like. In general, lithium salt electrolytes exhibit a low transference number of lithium ions (0.3~0.5/l), which results in poor high-rate performances and limits the powder output of the cell [1] because of

their dielectric mechanism such as solvation and dissociation. However, the most important things to address are safety related to thermal stability and leakage of the liquid type. As the organic electrolyte is decomposed and high thermal energy is generated at high temperature, the lithium batteries expand and induce membrane shrinkage. And finally, the short circuit occurs between the cathode and the anode, causing an explosion. To solve these problems, various types of electrolytes such as gel-type and solid state electrolytes having no leakage and excellent thermal and electrochemical stability have been developed.
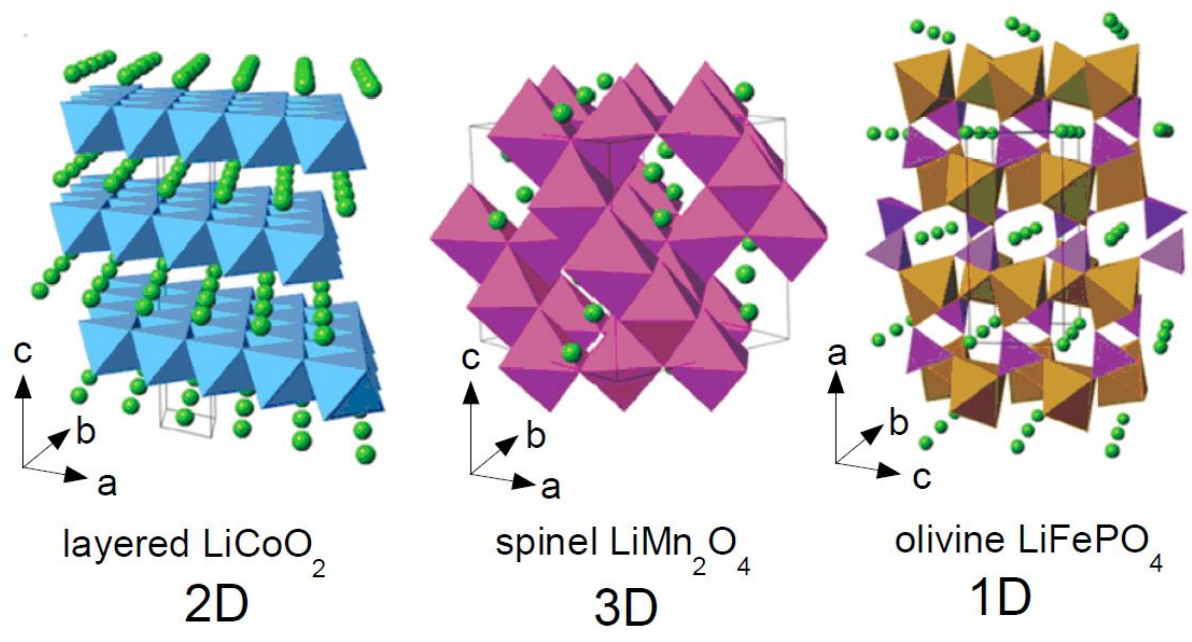
Figure 1.1. Crystal structures of the three lithium-insertion compounds in which the Li$^+$ ions are mobile through the 2-D (layered), 3-D (spinel) and 1-D (olivine) frameworks.
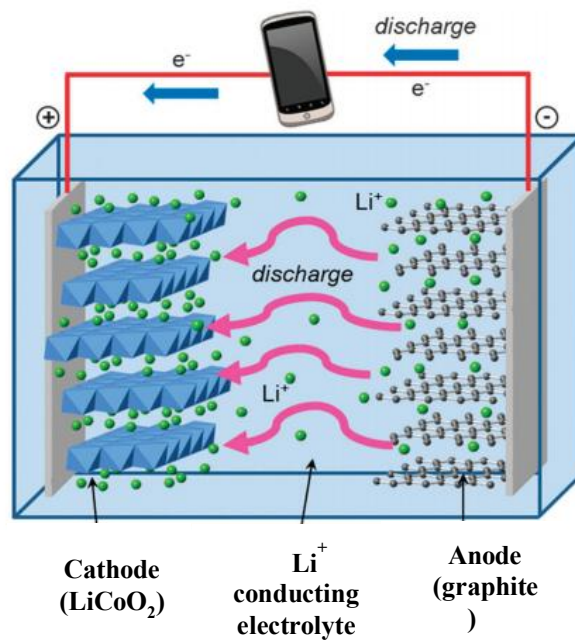
Figure 1.2. Illustration of operating principle of lithium secondary battery system.
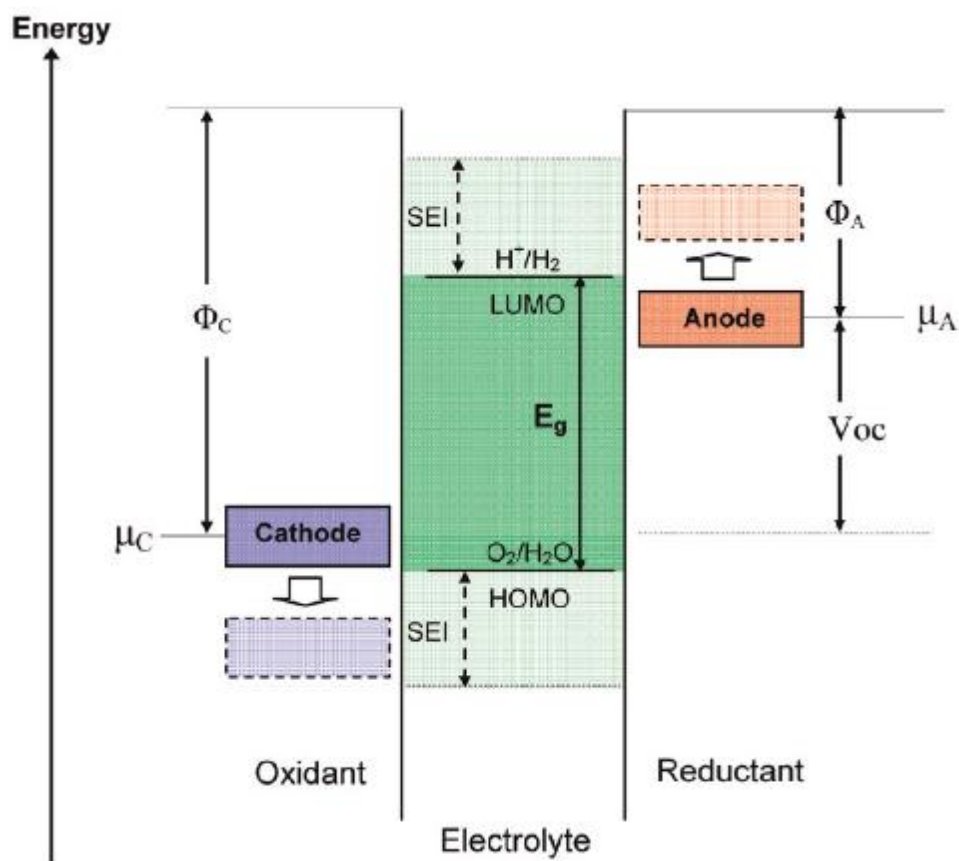
Figure 1.3. Schematic open-circuit energy diagram of a lithium cell.

1-2. All-solid-state lithium ion batteries

Lithium-ion batteries have been widely used as rechargeable power sources for portable electronics and large-scale devices such as mobile phones, laptops, and hybrid electronic vehicles [5]. Conventional organic liquid electrolytes, commonly used in lithium- ion batteries, have serious problems due to their risk of leakage and flammability [6]. Therefore, replacing liquid electrolytes with solid electrolytes could improve the electrochemical performance, safety, and reliability of these batteries as well as provide higher energy densities [7]. In addition, solid electrolytes have received much attention due to their potential for good ionic conductivity and a high lithium transference number (~1) compared to aprotic electrolytes (0.2~0.5) [8, 9]. Among these advantages, the solid electrolytes for large scale electric devices have been intensively studied due to their attractive advantages in safety such as electrochemical and thermal stability in lithium secondary batteries [1, 2]. The solid electrolytes are largely divided into inorganic materials and polymers. In the case of polymer electrolytes, they have good flexibility and can also be flexible batteries and devices. However, the poor mechanical properties and low ionic conductivity make these electrolytes out of practical application. Therefore, many researchers have been studying inorganic solid electrolytes.

1-2-1. Inorganic/ceramic solid electrolyte

Compare with the polymer electrolytes, inorganic solid electrolytes have been actively studied because of their excellent safety, including strong mechanical strength and good ionic conductivity. There are many types of electrolytes such as lithium hydride, perovskite, lithium nitride, LISICON-like (lithium superionic conductor), NASICON-like (sodium superionic conductor), argyrodite, and garnet [10].

1-2-2. Properties of inorganic/ceramic solid electrolyte

Before commercialization, the inorganic solid electrolytes meet the following requirements:

1)   Strong mechanical strength

2)   Chemical stability from thermal decomposition [11] and flammable [12]

3)   High ionic conductivity due to high lithium transference number (~1)

        compared to aprotic electrolytes (0.2-0.5) [8]

4)   Stable electrochemical stability window [13]

5)   Good compatibility with lithium metal batteries due to its Li dendrite

        suppression properties [14]

6)   Eco-friendly comparing with organic carbonate base electrolytes

Inorganic electrolytes almost satisfy mechanical strength, chemical stability, nonflammable, Li dendrite suppression, and eco-friendly. In particular, the improved stability and safety of inorganic solid electrolytes can easily and simply provide new designs of all-solid-state battery cells. Moreover, the solid electrolytes have high lithium transference number ($\sigma_{Li}/\sigma_{total}$), which reduces the effect of concentration polarization by precipitation of dissolved salts in the anode and depletion at the cathode [8], compared to liquid electrolytes containing aprotic and lithium salt ions, because they operate only by Li$^+$ migration. Consequently, the lifetime and safety of lithium ion batteries are increased [10]. The electrochemical stability window of many inorganic electrolytes is known to be stable and wide. Almost the oxide electrolytes showed stable cathodic stability at the voltage window of the cathode (5~9V versus Li$^+$/Li) and did not induce self-decomposition during charging and discharging, unlike the liquid organic electrolytes [8]. As a result, the solid electrolyte can suppress the repetition of SEI formation and Li$^+$ consumption, and finally increase the lifetime of lithium secondary batteries.

1-2-3. Li$^+$ diffusion mechanism of inorganic/ceramic solid electrolyte

Inorganic solid electrolytes are composed of mobile ions such as Li$^+$, as well as non-metallic ligands and central metals that constitute the polyhedron (4, 6, 8, and 12-fold

coordination) forming the framework of the crystal structures. Polyhedrons are ordered regularly by sharing such as corner or edge sharing, and form the Li^+ tunnels called bottlenecks with interstitials between large anions and vacancy from incomplete crystallinity of the solid material due to thermodynamic stabilization [8, 15]. In the solid electrolytes, the lithium ions are diffused by migration through bottlenecks of the crystal structure, whereas liquid electrolytes involve the movement of solvated lithium ions in a solvent medium [8]. The migration divided into Schottky migration and Frenkel migration. In the case of Schottky migration, lithium ions move randomly to vacancies. In contrast, Frenkel migration occurs when lithium ions diffuse directly into the interstitial between the anions and the exchange interstitial sites [10]. When comparing the activation energy of migration, the Frenkel migration mechanism requires lower activation energy than Schottky migration. As a result, the Li^+ conductivity depends on the size and number of bottlenecks [16]. Interstitial and vacancy sites depend on the lattice parameters of the unit cell in structures with Li^+ concentrations. Also, the parameters are changed by the valence and size of the mobile ion [8]. For example, the repulsion between the same charge ions increases with increasing ion size and creates a larger bottleneck size and interstitial. For the ionic valence effect, the ionic conductivity decreases with increasing valence because the electrostatic interaction between the mobile ion and the counter-charged ion increases and ionic diffusion decreases.

1-3. Inorganic electrolyte

1-3-1. Oxide solid electrolyte

Oxide-based solid electrolytes for all-solid-state batteries have low ionic conductivity, however, good chemical and mechanical stability, and in particular, many studies have been conducted due to their stability in the atmosphere. Most oxide-based solid electrolytes produced have focused on using NASICON, perovskite, garnet, and LISICON structures.

NASICON-like structures are generally known as a rhombohedral unit cell and $R\bar{3}c$ with a few monoclinic and orthorhombic phases [17]. Representatively, $L_{1+6x}M_{4+2-x}M'_{3+x}(PO_4)_3$ phosphates (L = Li or Na and M =Ti, Ge, Sn, Hf, or Zr and M' = Cr, Al, Ga, Sc, Y, In, or La) are composed with MO_6 octahedra connected by corner sharing with PO_4 tetrahedral to form

3D interconnected channels and two types of interstitial positions where mobile cations are distributed [18]. The M1 sites which are 6-fold coordination located between two MO_6 octahedral while M2 sites that are 8-fold coordinated and located between two columns of MO_6 octahedral [19]. The lithium ions diffuse from on site to another through bottlenecks. However, the NASICON electrolytes containing Ti are unstable with Li metal at low potentials [20].

Perovskite materials having chemical formula ABO_3 is well known as the representative cubic phase with space group $Pm\overline{3}m$. Among the structural materials, lithium-lanthanum-titanates, $Li_{3x}La_{2/(3-x)}TiO_3$ (LLTO), is representative material due to its high ionic conductivity at room temperature (10^{-3} S/cm) [10]. The A site cations, which were Li^+ and La^{3+} in the cubic α-phase, were randomly distributed, while the A sites of the ordered β-LLTO had a doubled perovskite structure, with an alternating arrangement of La^+ rich and Li vacancy rich layers along the c axis [21]. Not only high ionic conductivity, the materials have many advantages such as stability in air and moisture, wide stability temperature window (to 1600K), good electrochemical stability (>8V). However, the materials have difficult to applied to commercial solid battery system because of its unsuitable for use with lithium and graphite negative electrodes [3, 10], high temperature sintering for synthesis and lower ionic conductivity than single crystal due to blocking grain boundaries [22].

The garnets exhibit a general chemical formula of $A_3B_2(XO_4)_3$ (A = Ca, Mg, Y, La or rare earth; B = Al, Fe, Ga, Ge, Mn, Ni or X = Si, Ge, Al) where A, B and C are eight, six and four oxygen coordinated cation sites, which crystalize in a face centered cubic structure with the space group $Ia\overline{3}d$ [23]. Because the garnet electrolytes high Li^+ concentration 5~7 Li atoms per formula unit and can accommodate excess Li^+ at octahedral sites than that of number of lithium at the tetrahedral sites [23], the ionic conductivity of the electrolytes can be controlled by increasing Li concentration. For example, $Li_5La_3M_2O_{12}$ have low ionic conductivity of 10^{-6} S/cm at room temperature. However, the low conductivity can be improved by substituting La and M sites with cations in an oxidation state higher or lower than La^{3+} and M^{5+} controlling the content of substitution elements such as $Li_{6.6}La_3Zr_{1.6}Sb_{0.4}O_{12}$ (7.7×10^{-4} S/cm) and $Li_{6.2}La_3Zr_{1.2}Sb_{0.8}O_{12}$ (4.5×10^{-4} S/cm) [24, 25]. Also, ionic conductivity of the garnet electrolytes can be improved by controlling shape control. For example, the particle shape of $Li_7La_3Zr_2O_{12}$ changes by contents of substitution element (Ga), and can be more dense pellets

with same pressure [26]. As the results, the interface resistance by grain boundary was reduced. Although garnet electrolytes have high lithium concentration and ionic conductivity, the materials couldn`t be commercialized because of their unstable reactivity with cathode materials at the positive voltage window [27].

The crystal structure of LISICON-like compounds is related to the γ-Li_3PO_4 structure with orthorhombic unit cell and *pnma* space group, where all cations are tetrahedral coordinated [10, 28]. The oxide LISICON-like materials such as $Li_{14}ZnGe_4O_{16}$ showed low ionic conductivity ($\sim 10^{-7}$ S/cm) at room temperature by trapping of the mobile Li^+ ions by the immobile sublattice at lower temperatures via the formation of defect complexes [20]. And the LISICON structures such as $Li_{3x}La_{2/3-x}TiO_3$ and $Li_{3/8}Sr_{7/16}Zr_{1/4}Ta_{3/4}O_3$, have low contact with Li metal due to the reduction of Ti and Ta ions.

Recently, thio-LISICON, which has been changed from O^{2-} to S^{2-} have been studied for high lithium ion conductivity at room temperature [10]. Many thio materials such as $Li_{10}MP_2S_{12}$ (M= Si, Ge, and Sn), $Li_{11}Si_2PS_{12}$ showed high ionic conductivity [29-31]. Especially, $Li_{10}GeP_2S_{12}$ showed highest lithium ion conductivity ($\sim 10^{-2}$ S/cm) at 27℃ [29] among current ceramic electrolytes [10]. As the radius of S^{2-} is higher than O^{2-}, this substitution can significantly enlarge the size of Li^+ transport bottlenecks. Also, S^{2-} has better polarization capability than O^{2-}. Consequently, the interaction between skeleton and Li^+ ion is weaker and make the mobility of Li^+ [32]. The thio-LISICON materials also have favorable advantage, which is reduction of grain boundary resistance by simple cold-press of electrolytes powders because of its good ductility compare with hard oxide materials [20].
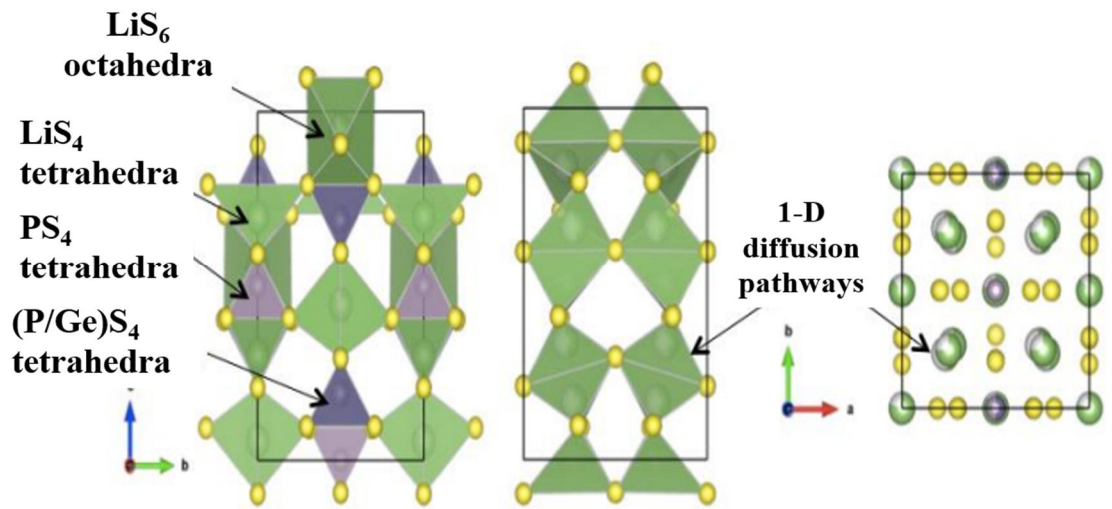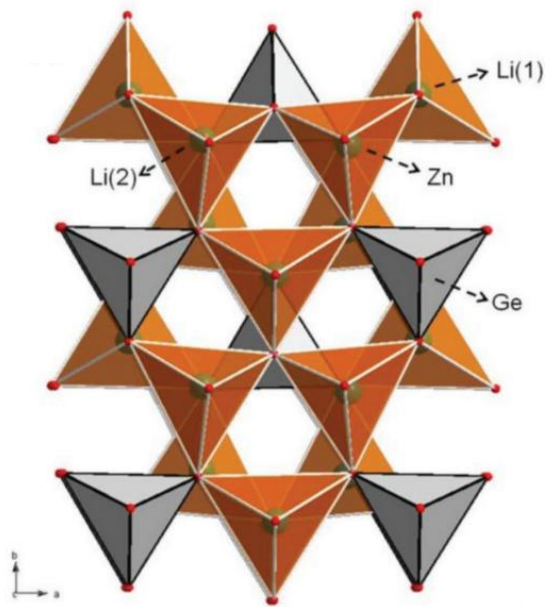
Figure 1.4. Schematic structure of LISICON-like.

1-3-2. Sulfide solid electrolyte

Sulfide-based solid electrolytes have a smaller grain boundary and easy to process because they have a good ductility. However, since sulfide-based solid electrolytes react with moisture in the atmosphere to generate hydrogen sulfide gas, all processes must be performed in an environment where moisture is blocked. Nevertheless, the sulfide-based solid electrolytes have higher ionic conductivity than the oxide-based electrolytes because they have low binding strength with lithium ions due to the high polarizability and low electronegativity of sulfur ions compared to oxygen ions [33, 34]. Since the ionic radius of the S^{2-} is bigger than that of the O^{2-}, the ion migration channel is larger, so the ion mobility is also greater [35]. Representative sulfide-based solid electrolytes currently being studied include thio-LISICON, Li_2S-P_2S_5 (LPS), and Li-argyrodite.

1-3-2-1. Thio-LISICON

Thio-LISICON materials such as $Li_{3.25}Ge_{0.25}P_{0.75}S_4$ and $Li_{10}GeP_2S_{12}$ were known that the materials have theoretical wide electrochemical stability window from 0V to 4V versus Li/Li^+ [36]. However, many results have been explained that the sulfide materials have narrow electrochemical window and react with cathode and anode [20, 31, 37, 38]. Because of the larger size and smaller electronegativity of S^{2-} than O^{2-}, the chemical interaction in the crystals structure of thio-materials is weak. As the results, the materials composed with S^{2-} anion have similar stability of less than 25meV per atom and show unstable characteristic than oxide materials. In the LGPS system, the $Li_{10}GeP_2S_{12}$ electrolyte received a lot of attention due to its lithium ion conductivity of 10^{-2} S/cm or more. However, since the amount of Ge in nature is limited, research to substitute Ge with other elements is still in progress. Actually, almost thio-materials react and are decomposed with cathode materials and anode materials including Li metal [38, 39]. In addition, the materials are difficult to synthesis at general atmosphere because they are very sensitive to air and moisture.

1-3-2-2. Li_2S-P_2S_5

Li_2S-P_2S_5 based glass-ceramics are of special interest due to their high ionic conductivity up to 1.7×10^{-2} S/cm at room temperature and their wide electrochemical window [40-44].

The Li$_2$S-P$_2$S$_5$ electrolyte is a metastable glass-ceramics with a (100-x)Li$_2$S-xP$_2$S$_5$ composition. This metastable phase is formed through partial crystallization by heat treatment after formation of the glass electrolyte. According to each composition ratio, these metastable phases such as Li$_7$P$_3$S$_{11}$, β-Li$_3$PS$_4$, and thio-LISICON analog showed higher lithium ion conductivity than Li$_4$P$_2$S$_6$ which is the stable crystalline phase. Among them, Li$_7$P$_3$S$_{11}$ (LPS) glass-ceramic can be easily synthesized by methods such as ball milling and solution techniques that allow other components to be mixed with the LPS [45, 46]. The Li$_7$P$_3$S$_{11}$ electrolyte which has a composition ratio of Li$_2$S and P$_2$S$_5$ of 7:3 reduced the interfacial resistance through hot press and exhibited lithium ion conductivity of 10^{-2} S/cm. Moreover, the powder obtained after heat treatment can be easily applied to the fabrication of electrolytes for bulk type ASSLBs [47]. However, since the LPS electrolyte is very unstable, it reacts with the lithium anode and decomposes, and the interfacial resistance with lithium metal is large. Due to the reaction characteristics between LPS and Li metal, low coulombic efficiency and capacity degradation in all-solid-state batteries are caused, which limits the application of all-solid-state batteries [45].

1-3-2-3. Argyrodite

Argyrodite is a class of chalcogenide structures related to Ag$_8$GeS$_6$ minerals that include various fast Ag$^+$ or Cu$^+$ ion conductors, such as A$_7$PS$_5$X (A = Ag$^+$, Cu$^+$). Recently, Deiseroth et al. synthesized the analogue cubic Li$^+$ argyrodite with the formula Li$_6$PS$_5$X (X=Cl, Br, I) and Li$_7$PS$_6$. The Li-argyrodite electrolyte is a lithium conductor having a structure similar to that of Ag$_8$GeS$_6$ which has a mineral argyrodite structure. The Li-argyrodite electrolyte has a structure in which silver ions in a mineral argyrodite structure are replaced with lithium ions because the atomic radius of silver ions and lithium ions are similar and have the same coordination number. And ion diffusion proceeds through a specific atomic position that is irregularly generated [48, 49].
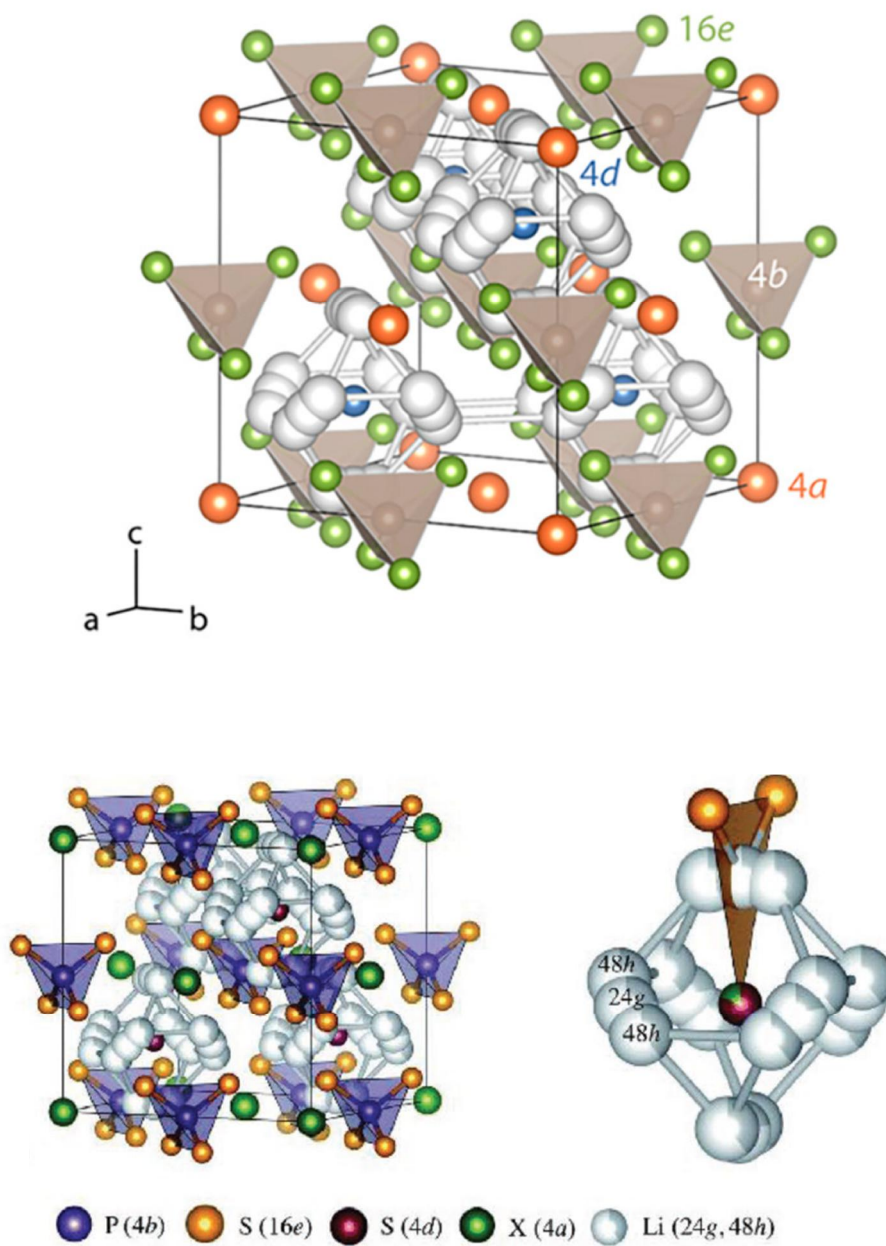
Figure 1.5. Crystal structure of argyrodite-type Li_6PS_5X.

1-4. Sulfide solid electrolyte/oxide cathode interface

Oxide cathodes containing lithium transition metal oxides and phosphates have been widely used in commercial lithium-ion batteries due to their high electrochemical potential and large capacity. The combination of sulfide electrolyte and oxide cathode could enable the development of new all-solid-state lithium batteries (ASSLBs) with high safety and energy density. However, the interfacial instability between the sulfide-based solid electrolyte and the oxide cathode limits its application in ASSLBs.

1-4-1. Problems of the interface between sulfide electrolyte/oxide cathode

Interdiffusion occurs when a solid is in contact with a solid. The degree of inter-diffusion depends on the mutual solubility and the diffusion coefficient of the composed mobile elements. Diffusion of ionic solids most often occurs during high-temperature processing or electrochemical cycling, as the diffusion of polyvalent ions is very slow at ambient conditions. In particular, a significant amount of interdiffusion is known to occur during electrochemical cycling of ASSLBs composed of high-voltage cathodes and sulfide-based solid electrolytes. As a solution, the inclusion of an interlayer such as a coating can mitigate this interdiffusion, thereby inhibiting degradation and preventing the formation of a resistive interface [50-53].

The space charge layer is formed at the interface between two ion conductors with significantly different lithium chemical potentials. This can lead to high interfacial resistance, which severely affects the fast charge-discharge capability of ASSLBs. Oxide cathodes are generally mixed conductors with high ionic and electronic conductivity, whereas sulfide electrolytes are single lithium ion conductors. Therefore, the contact between the oxide cathodes and the sulfide electrolytes causes lithium ions to migrate from the sulfide electrolytes to the oxide cathodes due to the large chemical potential difference, resulting in the formation of the space charge layer [54].

In addition, oxidation of sulfide-based solid electrolytes at high potentials is inevitable. This oxidative decomposition induces the growth of impedance [55], which rapidly causes the capacity fading of the ASSLBs. For this reason, sulfide-based solid electrolyte requires a coated cathode material that prevents the reaction between the solid electrolyte and the cathode active material to minimize oxidation of the solid electrolyte. And it should be taken into account that uncoated NCM materials are known to release oxygen during cycling, even

in the environment of ASSLBs. Additionally, elevated temperatures during electrochemical cycling can lead to interdiffusion and reaction of the cathode active material and the coating material. Therefore, in general, an ideal coating material should have low mobility for all ions other than lithium, and those ions, like large cations with a high positive charge, should exhibit a small diffusion coefficient in the cathode active material.

One of the reasons why $LiNbO_3$ functions well as a coating material is that Nb^{5+} cations do not rapidly diffuse into the cathode active material. Another reason for using compounds with highly positively charged cations (such as Nb^{5+}, Ta^{5+} and P^{5+}) is the oxidative stability of these phases and their low tendency to release oxygen at high potentials.

1-4-2. Interfacial engineering

Several ternary oxides (e.g. $LiNbO_3$, $Li_4Ti_5O_{12}$ and Li_2SiO_3) have already been studied as cathode active material coatings for ASSLBs to prevent degradation of solid electrolytes, reduce interfacial resistance, and improve specific capacity, rate capability and cycle life of batteries. Among them, $LiNbO_3$ is currently the most widely used coating material and $LiNbO_3$ has been established as a prototype coating material for improving ASSLBs performance. Amorphous $LiNbO_3$ shows an ionic conductivity of about 10^{-5} S·cm^{-1} and an electronic conductivity of less than 10^{-11} S·cm^{-1}, so it is suitable as a material for the interfacial buffer layer [56, 57].

The wet chemical approach, which is mainly used among various coating methods, provides the cheapest and simplest route for coating the cathode active material because it can be performed without the use of complicated or additional expensive equipment. However, the disadvantage is that it is difficult to control the thickness, shape and homogeneity of the coating [58].

Spray coating technically falls under the category of wet chemistry methods, but this method is unique and complex enough to separate it from the previous one. This approach has been very successful in obtaining uniform coatings of $LiNbO_3$ and $Li_4Ti_5O_{12}$ on the surface of anode materials such as $LiNi_{1-x-y}Co_xMn_yO_2$, $LiNi_{0.80}Co_{0.15}Al_{0.05}O_2$, $LiMn_2O_4$, and $LiCoO_2$ with various thicknesses, compositions and morphologies. And this has become somewhat of the standard coating procedure. However, the disadvantages of this approach use expensive equipment and the need to coat the cathode material in kilograms [59].

1-5. Purpose

As mentioned above, it is essential to use coated cathode active materials in the manufacture of ASSLBs due to the reaction at the interface between the cathode active material and the solid electrolyte, which affects the performance of the ASSLBs. Lithium niobate ($LiNbO_3$), a widely used representative coating material, requires an expensive precursor to be used in the coating process. And the coating method is also complicated and expensive, which hinders the commercialization of ASSLBs.

In order to solve this problem, instead of surface coating on the cathode active material, in this paper, $LiNbO_3$ was used as a precursor to produce a sulfide-based solid electrolyte, and this solid electrolyte was mixed with an uncoated cathode active material to make a composite cathode. Then, the ASSLB was manufactured using this composite cathode and solid electrolyte, and as a result, interfacial stability was improved.

Reference

[1] Minh, Nguyen Q. "Ceramic fuel cells." *Journal of the American Ceramic Society* 76, no. 3 (1993): 563-588.

[2] Tarascon, J-M., and Michel Armand. "Issues and challenges facing rechargeable lithium batteries." In *Materials for sustainable energy: a collection of peer-reviewed research and review articles from Nature Publishing Group*, pp. 171-179. 2011.

[3] Stephan, A. Manuel, and K. S. Nahm. "Review on composite polymer electrolytes for lithium batteries." *Polymer* 47, no. 16 (2006): 5952-5964.

[4] Xu, Kang. "Nonaqueous liquid electrolytes for lithium-based rechargeable batteries." *Chemical reviews* 104, no. 10 (2004): 4303-4418.

[5] Seino, Yoshikatsu, Tsuyoshi Ota, Kazunori Takada, Akitoshi Hayashi, and Masahiro Tatsumisago "A sulphide lithium super ion conductor is superior to liquid ion conductors for use in rechargeable batteries" Energy & Environmental Science 7, no. 2 (2014): 627-631.

[6] Zhang, Jicheng, Rui Gao, Limei Sun, Heng Zhang, Zhongbo Hu, and Xiangfeng Liu "Unraveling the multiple effects of Li_2ZrO_3 coating on the structural and electrochemical performances of $LiCoO_2$ as high-voltage cathode materials" *Electrochimica Acta* 209 (2016): 102-110.

[7] Wenzel, Sebastian, Dominik A. Weber, Thomas Leichtweiss, Martin R. Busche, Joachim Sann, and Jürgen Janek "Interphase formation and degradation of charge transfer kinetics between a lithium metal anode and highly crystalline $Li_7P_3S_{11}$ solid electrolyte." *Solid State Ionics* 286 (2016): 24-33.

[8] Xu, Kang "Nonaqueous liquid electrolytes for lithium-based rechargeable batteries" *Chemical Reviews* 104, no. 10 (2004): 4303-4418.

[9] Kamaya, Noriaki, Kenji Homma, Yuichiro Yamakawa, Masaaki Hirayama, Ryoji Kanno, Masao Yonemura, Takashi Kamiyama, Yuki Kato, Shigenori Hama, Koji Kawamoto and

Akio Mitsui "A lithium superionic conductor" *Nature Materials* 10, no. 9 (2011): 682.

[10] Bachman, John Christopher, Sokseiha Muy, Alexis Grimaud, Hao-Hsun Chang, Nir Pour, Simon F. Lux, Odysseas Paschos et al. "Inorganic solid-state electrolytes for lithium batteries: mechanisms and properties governing ion conduction." *Chemical reviews* 116, no. 1 (2016): 140-162.

[11] Goodenough, John B., and Youngsik Kim. "Challenges for rechargeable Li batteries." *Chemistry of materials* 22, no. 3 (2010): 587-603.

[12] Dyer, Chris K., Patrick T. Moseley, Zempachi Ogumi, David AJ Rand, and Bruno Scrosati, eds. *Encyclopedia of Electrochemical Power Sources*. Elsevier Science & Technology., 2009.

[13] Jung, Yun-Chae, Seul-Ki Kim, Moon-Sung Kim, Jeong-Hye Lee, Man-Seok Han, Duck-Hyun Kim, Woo-Cheol Shin, Makoto Ue, and Dong-Won Kim. "Ceramic separators based on Li$^+$-conducting inorganic electrolyte for high-performance lithium-ion batteries with enhanced safety." *Journal of Power Sources* 293 (2015): 675-683.

[14] Garche, Jurgen, Chris K. Dyer, Patrick T. Moseley, Zempachi Ogumi, David AJ Rand, and Bruno Scrosati, eds. *Encyclopedia of electrochemical power sources*. Newnes, 2013.

[15] A. Martínez-Juárez, C. Pecharromán, J. E. Iglesias, and J. M. Rojo, "Relationship between activation energy and bottleneck size for Li$^+$ ion conduction in NASICON materials of composition LiMM′(PO$_4$)$_3$; M, M′ = Ge, Ti, Sn, Hf," *J. Phys. Chem. B*, vol. 102, no. 2, pp. 372–375, 1998.

[16] J. B. Goodenough, "Oxide-ion electrolytes," *Annu. Rev. Mater. Res.*, vol. 33, pp. 91–128, 2003.

[17] Aono, Hiromichi, Eisuke Sugimoto, Yoshihiko Sadaoka, Nobuhito Imanaka, and Gin-ya Adachi. "The electrical properties of ceramic electrolytes for LiMxTi$_{2-x}$(PO$_4$)$_{3+y}$Li$_2$O, M= Ge, Sn, Hf, and Zr systems." *Journal of The Electrochemical Society* 140, no. 7 (1993): 1827-1833.

[18] Ortiz, Gregorio F., María C. López, Pedro Lavela, Candela Vidal-Abarca, and José L.

Tirado. "Improved lithium-ion transport in NASICON-type lithium titanium phosphate by calcium and iron doping." *Solid State Ionics* 262 (2014): 573-577.

[19] Norhaniza, R., R. H. Y. Subban, and N. S. Mohamed. "Cr and V substituted LiSn2P3O12 solid electrolyte materials." *Journal of power sources* 244 (2013): 300-305.

[20] Cao, Can, Zhuo-Bin Li, Xiao-Liang Wang, Xin-Bing Zhao, and Wei-Qiang Han. "Recent advances in inorganic solid electrolytes for lithium batteries." *Frontiers in Energy Research* 2 (2014): 25.

[21] Hartmann, Pascal, Thomas Leichtweiss, Martin R. Busche, Meike Schneider, Marisa Reich, Joachim Sann, Philipp Adelhelm, and Jürgen Janek. "Degradation of NASICON-type materials in contact with lithium metal: formation of mixed conducting interphases (MCI) on solid electrolytes." *The Journal of Physical Chemistry C* 117, no. 41 (2013): 21064-21074.

[22] Wenzel, Sebastian, Thomas Leichtweiss, Dominik Krüger, Joachim Sann, and Jürgen Janek "Interphase formation on lithium solid electrolytes-An in situ approach to study interfacial reactions by photoelectron spectroscopy." *Solid State Ionics* 278 (2015): 98-105.

[23] Thangadurai, Venkataraman, Sumaletha Narayanan, and Dana Pinzaru. "Garnet-type solid-state fast Li ion conductors for Li batteries: critical review." *Chemical Society Reviews* 43, no. 13 (2014): 4714-4727.

[24] Cussen, Edmund J. "Structure and ionic conductivity in lithium garnets." *Journal of Materials Chemistry* 20, no. 25 (2010): 5167-5173.

[25] Ramakumar, S., L. Satyanarayana, Sunkara V. Manorama, and Ramaswamy Murugan. "Structure and Li+ dynamics of Sb-doped $Li_7La_3Zr_2O_{12}$ fast lithium ion conductors." *Physical Chemistry Chemical Physics* 15, no. 27 (2013): 11327-11338.

[26] El Shinawi, Hany, and Jürgen Janek. "Stabilization of cubic lithium-stuffed garnets of the type "$Li_7La_3Zr_2O_{12}$" by addition of gallium." *Journal of power sources* 225 (2013): 13-19.

[27] Kim, Ki Hyun, Yasutoshi Iriyama, Kazuo Yamamoto, Shota Kumazaki, Toru Asaka, Kinuka Tanabe, Craig AJ Fisher, Tsukasa Hirayama, Ramaswamy Murugan, and Zempachi Ogumi. "Characterization of the interface between $LiCoO_2$ and $Li_7La_3Zr_2O_{12}$ in an all-solid-state rechargeable lithium battery." *Journal of Power Sources* 196, no. 2 (2011): 764-767.

[28] West, A. R. "Crystal chemistry of some tetrahedral oxides." *Zeitschrift für Kristallographie-Crystalline Materials* 141, no. 1-6 (1975): 422-436.

[29] Bron, Philipp, Sebastian Johansson, Klaus Zick, Jörn Schmedt auf der Günne, Stefanie Dehnen, and Bernhard Roling. "$Li_{10}SnP_2S_{12}$: an affordable lithium superionic conductor." *Journal of the American Chemical Society* 135, no. 42 (2013): 15694-15697.

[30] Kamaya, Noriaki, Kenji Homma, Yuichiro Yamakawa, Masaaki Hirayama, Ryoji Kanno, Masao Yonemura, Takashi Kamiyama et al. "A lithium superionic conductor." *Nature materials* 10, no. 9 (2011): 682-686.

[31] Kuhn, Alexander, Oliver Gerbig, Changbao Zhu, Frank Falkenberg, Joachim Maier, and Bettina V. Lotsch. "A new ultrafast superionic Li-conductor: ion dynamics in $Li_{11}Si_2PS_{12}$ and comparison with other tetragonal LGPS-type electrolytes." *Physical Chemistry Chemical Physics* 16, no. 28 (2014): 14669-14674.

[32] Murayama, Masahiro, Ryoji Kanno, Michihiko Irie, Shinya Ito, Takayuki Hata, Noriyuki Sonoyama, and Yoji Kawamoto. "Synthesis of new lithium ionic conductor thio-LISICON—lithium silicon sulfides system" *Journal of Solid State Chemistry* 168, no. 1 (2002): 140-148.

[33] Muramatsu, Hiromasa, Akitoshi Hayashi, Takamasa Ohtomo, Sigenori Hama, and Masahiro Tatsumisago "Structural change of $Li_2S–P_2S_5$ sulfide solid electrolytes in the atmosphere" *Solid State Ionics* 182, no. 1 (2011): 116-119.

[34] Ohtomo, Takamasa, Akitoshi Hayashi, Masahiro Tatsumisago, and Koji Kawamoto "Suppression of H_2S gas generation from the $75Li_2S\cdot25P_2S_5$ glass electrolyte by additives" *Journal of Materials Science* 48, no. 11 (2013): 4137-4142.

[35] Tatsumisago, Masahiro, and Akitoshi Hayashi "Sulfide Glass-Ceramic Electrolytes for All Solid-State Lithium and Sodium Batteries" *International Journal of Applied Glass Science* 5, no. 3 (2014): 226-235.

[36] Kanno, Ryoji, and Masahiro Murayama. "Lithium ionic conductor thio-LISICON: the $Li_2SGeS_2P_2S_5$ system." *Journal of the electrochemical society* 148, no. 7 (2001): A742-A746.

[37] Rao, R. Prasada, and S. Adams. "Studies of lithium argyrodite solid electrolytes for all-solid-state batteries." *physica status solidi (a)* 208, no. 8 (2011): 1804-1807.

[38] Mo, Yifei, Shyue Ping Ong, and Gerbrand Ceder. "First principles study of the $Li_{10}GeP_2S_{12}$ lithium super ionic conductor material." *Chemistry of Materials* 24, no. 1 (2012): 15-17.

[39] Chung, Habin, and Byoungwoo Kang. "Increase in grain boundary ionic conductivity of $Li_{1.5}Al_{0.5}Ge_{1.5}(PO_4)_3$ by adding excess lithium." *Solid State Ionics* 263 (2014): 125-130.

[40] Liu, D., W. Zhu, Z. Feng, A. Guerfi, A. Vijh, and K. Zaghib "Recent progress in sulfide-based solid electrolytes for Li-ion batteries" *Materials Science and Engineering: B* 213 (2016): 169-176.

[41] Che, Haiying, Suli Chen, Yingying Xie, Hong Wang, Khalil Amine, Xiao-Zhen Liao, and Zi-Feng Ma "Electrolyte design strategies and research progress for room-temperature sodium-ion batteries" *Energy & Environmental Science* 10, no.5 (2017): 1075-1101.

[42] Chen, Long, Yutao Li, Shuai-Peng Li, Li-Zhen Fan, Ce-Wen Nan, and John B. Goodenough "PEO/garnet composite electrolytes for solid-state lithium batteries: from "ceramic-in-polymer" to "polymer-in-ceramic"" *Nano Energy* 46 (2018): 176-184.

[43] Owejan, Jeanette E., Jon P. Owejan, Steven C. DeCaluwe, and Joseph A. Dura "Solid electrolyte interphase in Li-ion batteries: evolving structures measured in situ by neutron reflectometry" *Chemistry of Materials* 24, no. 11 (2012): 2133-2140.

[44] Tan, Guoqiang, Feng Wu, Chun Zhan, Jing Wang, Daobin Mu, Jun Lu, and Khalil Amine

"Solid-state li-ion batteries using fast, stable, glassy nanocomposite electrolytes for good safety and long cycle-life" *Nano Letters* 16, no. 3 (2016): 1960-1968.

[45] Mo, Shanshan, Penghao Lu, Fei Ding, Zhibin Xu, Jiaquan Liu, Xingjiang Liu, and Qiang Xu "High-temperature performance of all-solid-state battery assembled with 95(0.7 Li_2S-0.3 P_2S_5)-5Li_3PO_4 glass electrolyte" *Solid State Ionics* 296 (2016): 37-41.

[46] Ohtomo, Takamasa, Akitoshi Hayashi, Masahiro Tatsumisago, Yasushi Tsuchida, Shigenori Hama, and Koji Kawamoto "All-solid-state lithium secondary batteries using the 75$Li_2S \cdot 25P_2S_5$ glass and the 70$Li_2S \cdot 30P_2S_5$ glass–ceramic as solid electrolytes" *Journal of Power Sources* 233 (2013): 231-235.

[47] Lü, Xujie, John W. Howard, Aiping Chen, Jinlong Zhu, Shuai Li, Gang Wu, Paul Dowden, Hongwu Xu, Yusheng Zhao, and Quanxi Jia "Antiperovskite Li_3OCl Superionic Conductor Films for Solid-State Li-Ion Batteries" *Advanced Science* 3, no. 3 (2016): 1500359.

[48] R. B. Beeken, J. J. Garbe, J. M. Gillis, N. R. Petersen, B. W. Podoll, and M. R. Stoneman, "Electrical conductivities of the Ag_6PS_5X and the Cu_6PSe_5X (X=Br, I) argyrodites," *J. Phys. Chem. Solids*, vol. 66, no. 5, pp. 882–886, 2005.

[49] H.-J. Deiseroth *et al.*, "Li_6PS_5X: A Class of Crystalline Li-Rich Solids With an Unusually High Li^+ Mobility," *Angew. Chemie*, vol. 120, no. 4, pp. 767–770, 2008.

[50] Nie, K., Hong, Y., Qiu, J., Li, Q., Yu, X., Li, H., & Chen, L. Interfaces Between Cathode and Electrolyte in Solid State Lithium Batteries: Challenges and Perspectives. *Frontiers in Chemistry* **2018**, 6. doi:10.3389/fchem.2018.00616.

[51] Zhang, W., Weber, D. A., Weigand, H., Arlt, T., Manke, I., Schröder, D, Janek, Interfacial Processes and Influence of Composite Cathode Microstructure Controlling the Performance of All-Solid-State Lithium Batteries. *ACS Applied Materials & Interfaces* **2017**, 9(21), 17835–17845. doi:10.1021/acsami.7b01137.

[52] Xu, L., Tang, S., Cheng, Y., Wang, K., Liang, J., Liu, C, Mai, L. Interfaces in Solid-State Lithium Batteries. *Joule* **2018**. doi:10.1016/j.joule.2018.07.009.

[53] Zuo, D., Tian, G., Li, X., Chen, D., & Shu, K. Recent progress in surface coating of cathode materials for lithium ion secondary batteries. *Journal of Alloys and Compounds* **2017**, 706, 24–40. doi:10.1016/j.jallcom.2017.02.230.

[54] Pervez, S. A., Cambaz, M. A., Thangadurai, V., & Fichtner, M. Interface in Solid-State Li Battery: Challenges, Progress and Outlook. *ACS Applied Materials & Interfaces* **2019**. doi:10.1021/acsami.9b02675.

[55] Xiao, Y., Wang, Y., Bo, S.-H., Kim, J. C., Miara, L. J., & Ceder, G. Understanding interface stability in solid-state batteries. *Nature Reviews Materials* **2019**, 5(2), 105–126. doi:10.1038/s41578-019-0157-5.

[56] Li, C., Zhang, H. P., Fu, L. J., Liu, H., Wu, Y. P., Rahm, H. Q. Cathode materials modified by surface coating for lithium ion batteries. *Electrochimica Acta* **2006**, 51(19), 3872–3883. doi:10.1016/j.electacta.2005.11.01.

[57] Gurung, A., Pokharel, J., Baniya, A., Pathak, R., Chen, K., Lamsal, B. S. A Review on Strategies Addressing Interface Incompatibilities in Inorganic All-Solid-State Lithium Batteries. *Sustainable Energy & Fuels* **2019**. doi:10.1039/c9se00549h.

[58] Wu, J., Shen, L., Zhang, Z., Liu, G., Wang, Z., Zhou, D, Yao, X. All-Solid-State Lithium Batteries with Sulfide Electrolytes and Oxide Cathodes. *Electrochemical Energy Reviews* **2020**. doi:10.1007/s41918-020-00081-4.

[59] Wang, S., Fang, R., Li, Y., Liu, Y., Xin, C., Richter, F. H., & Nan, C.-W. Interfacial challenges for all-solid-state batteries based on sulfide solid electrolytes. *Journal of Materiomics* **2020**. doi:10.1016/j.jmat.2020.09.003.

Chapter 2. General experimental

2-1. Physical characterization

2-1-1. X-ray diffraction (XRD)

X-ray powder diffraction (XRD) is essential technique that uses the diffraction of X-rays on powder or microcrystalline samples for the study of crystal structures and those of volume. The most popular analysis method for structural changes by crystal structures and environments (atmosphere, temperature etc.) of the powder samples. It is based on constructive interference of monochromatic X-ray and a crystalline sample. Therefore, it is possible to figure out the shape of crystalline from the diffraction of a crystal in any direction, the structure of material is also contained in the forward scattering. The inorganic powders were usually used as the sample for the diffraction analysis. The samples were interacted with the incident X-ray beam as followed Bragg`s Law equation (Figure 2.1).

$$n\lambda = 2d_{hkl}\sin\theta_{hkl} \quad \text{(Bragg equation)} \quad (n=1, 2, 3\ldots) \tag{2.1}$$

where λ is frequency of incident beam, d is d-spacing, θ is the diffraction angles when the samples interact with incident beam, hkl is miller index. This law related the wavelength of electromagnetic radiation to the diffraction angle and the lattice spacing in a crystalline powder. The difference of path length between reflections on neighboring planes is $d_{hkl}sin\theta_{hkl}$. For example, the smaller the distance d-spacing, the larger the diffraction angle θ. When the wavelength λ increase, the diffraction angle θ increase. Because the difference of path length means the different interference between the diffraction wavelength, the angle is main scale for determining the crystals. From the equations, the d-spacing can be calculated by considering Miller indices and unit cell parameter it was related 7 types of crystal system. Figure 2.2 is the table of the crystal system and d-spacing [1, 2]. The crystals depend on three cell parameters (a, b, c) and three angles (α, β, γ). The crystals are different symmetries from the cubic crystal composed with three same parameter values and three 90 degrees angles to triclinic. According to the rotational symmetry, there are 14 different

Bravais Lattices in which similar points can be arranged in a three-dimensional space not 28 cases by French crystallographer August Bravais in 1848. The 14 Bravais Lattices are combined with 32-point group symmetries and finally, give the 230 space groups. This powerful analysis can be applied to almost inorganic materials which have quite electronic density except for low periodic number such as Li due to its low electronic density.
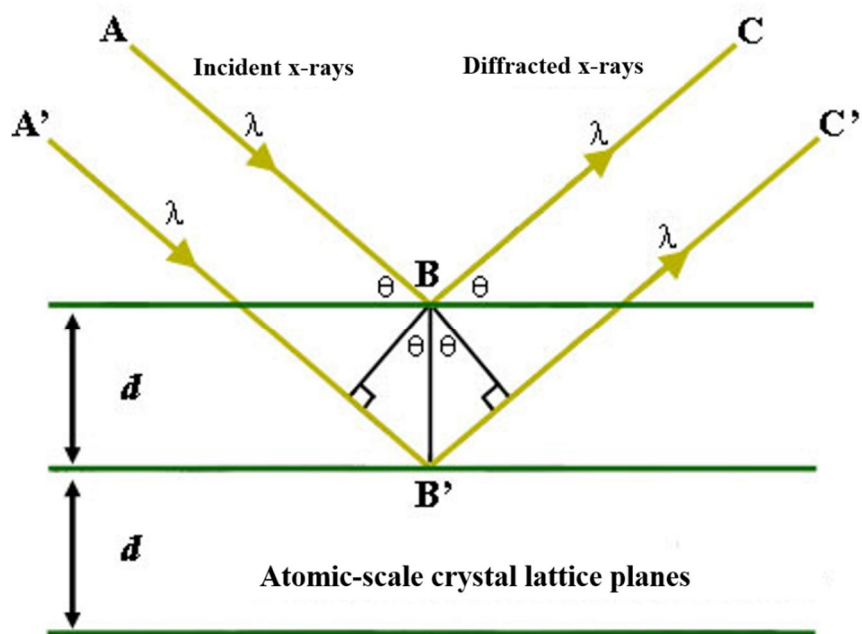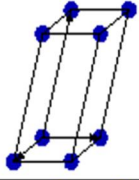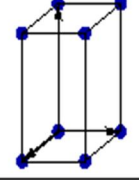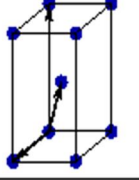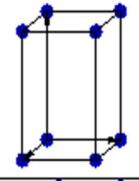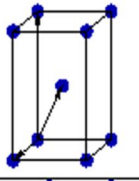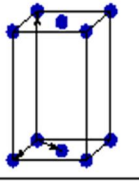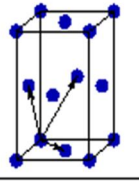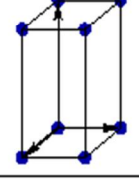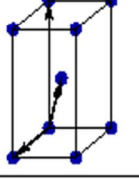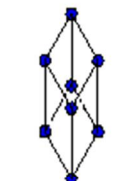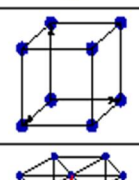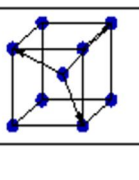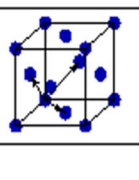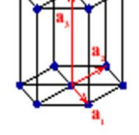
Figure 2.1. Bragg reflection on a set of atomic planes.

Table 2.1. 7 crystal system and 14 Bravais lattice.

Bravais lattice	Parameters	Simple (P)	Volume centered (I)	Base centered (C)	Face centered (F)
Triclinic	$a_1 \neq a_2 \neq a_3$ $\alpha_{12} \neq \alpha_{23} \neq \alpha_{31}$				
Monoclinic	$a_1 \neq a_2 \neq a_3$ $\alpha_{23} = \alpha_{31} = 90°$ $\alpha_{12} \neq 90°$				
Orthorhombic	$a_1 \neq a_2 \neq a_3$ $\alpha_{12} = \alpha_{23} = \alpha_{31} = 90°$				
Tetragonal	$a_1 = a_2 \neq a_3$ $\alpha_{12} = \alpha_{23} = \alpha_{31} = 90°$				
Trigonal	$a_1 = a_2 = a_3$ $\alpha_{12} = \alpha_{23} = \alpha_{31} < 120°$				
Cubic	$a_1 = a_2 = a_3$ $\alpha_{12} = \alpha_{23} = \alpha_{31} = 90°$				
Hexagonal	$a_1 = a_2 \neq a_3$ $\alpha_{12} = 120°$ $\alpha_{23} = \alpha_{31} = 90°$				

2-1-2. Filed emission scanning electron microscopy (FE-SEM)

FE-SEM is Field Emission Scanning Electron Microscope which operates with a high-energy electron beam in a scan pattern instead of light source. These electrons are released by a field emission source in a field emission gun. These electron emitters can produce up to 1000x the emission of a tungsten filament with high vacuum atmosphere to prevent unnecessary interaction between gas molecular and the electron beam. After the electrons beam exit the electron gun, monochromatic beam using metal apertures and magnetic lenses. And finally, the detectors of each type of electrons are placed in the microscopes that collect signals to produce an image of the patterns [3]. The electrons from the primary beam spread out in the sample to form the interaction volume. The size of the interaction volume depends on the accelerating voltage value of the primary electron beam and atomic number of the sample. The interaction volume increase with a larger accelerating voltage, but smaller for samples with a higher atomic number. Secondary electrons are produced from the surface of the sample or topmost part of the interaction volume and X-rays are generated within the whole of the interaction volume [4]. FE-SEM is used to visualized information of local area on the surface of chemicals. Also, the analysis can be combined with Energy dispersive X-ray spectroscopy (EDS) for good elemental analysis such as elemental composition near the surface of the samples with atomic number (Z)>3. The combination can also visualize the element distribution in a sample by mapping which showing the concentration of one element over a selected area of sample images. SEM-EDS mapping analysis is an effective elemental mapping which showing how to concentrate one element varies over an area of images of material.

2-1-3. Laser Raman spectroscopy

Raman spectroscopy is a spectroscopic technique typically used to determine vibrational modes of molecules, although rotational and other low-frequency modes of systems may also be observed. Raman spectroscopy is commonly used in chemistry to provide a structural fingerprint by which molecules can be identified. The light source used in Raman spectroscopy is a laser. The laser light is used because it is a very intense beam of nearly monochromatic light that can interact with sample molecules. When the radiation is absorbed, a molecule jumps to a higher vibrational or rotational energy level. Raman spectroscopy

relies upon inelastic scattering of photons, known as Raman scattering. A source of monochromatic light, usually from a laser in the visible, near infrared, or near ultraviolet range is used, although X-rays can also be used. The laser light interacts with molecular vibrations, phonons or other excitations in the system, resulting in the energy of the laser photons being shifted up or down. The shift in energy gives information about the vibrational modes in the system. Infrared spectroscopy typically yields similar, complementary, information. That's why we can detect structure of material using an excitation wavelength.

2-2. Electrochemical analysis

2-2-1. Electrochemical impedance spectroscopy (EIS)

Electrochemical impedance spectroscopy (EIS) is a powerful technique to measure the electrical impedance resistance of an electrode or whole cell system. The impedance of an electrochemical system is defined as the resistance when an AC voltage or current is applied over a range of frequencies. The current-voltage relationship of the impedance can be expressed as followed equation.

$$Z(w) = \frac{V(t)}{I(t)} = \frac{V_m sin(wt)}{I_m sin(wt-\theta)} = Z exp(j\theta)$$

Where v(t) and I(t) are AC voltage and current, Z(w) is impedance, w is frequency (w=2πf). The equation is derived by Euler's rule as below:

$$Z(w) = Z_{re} + iZ_{im}$$

Z_{re} and Z_{im} are the real and imaginary parts of the impedance in Nyquist plot which is one of the methods for expressing impedance like figure 2.3. From the obtained result, an equivalent circuit is deduced and is proved by the fitting procedure. The equivalent circuit gives the resistance component. For example, the real impedance value on x-axis from the O to initial value is mass transfer resistance considered as electrolyte resistance, the real value of the diameter of semicircle is charge transfer resistance related with a surface area of an electrode, and the Warburg region which is the tail is Warburg impedance related with lithium diffusion coefficient of an active material.

In the case of the solid electrolyte, the way to interpret the equivalent circuit is different. Fig 8 shows a suitable example for equivalent circuit of solid electrolyte. The real value from

0 to first semicircle means bulk resistance by a crystal structure and the insufficient contact between the particles of an active material and a solid electrolyte material. The second semicircle is the resistance by the grain boundary meaning a crack of solid electrolyte pellet. These factors are main resistance by solid electrolytes. The ionic conductivity of the solid electrolyte is calculated by below equation.

$$\sigma = \frac{l}{RA} = S/cm$$

Where l is thickness of a solid electrolyte pellet, R is the resistance, and A is the area of the pellet.

(a)

Double layer
capacitance
(C_{dl})

Solution
Resistance
(R_s)

Charge
transfer
Resistance
(R_{ct})

Diffusion
Warberg
impedance
(Z_W)

(b)

(c)

$$R_s + C_{dl} + R_{ct} + Z_w$$

C_{dl}

R_s

R_{ct}

Z_w
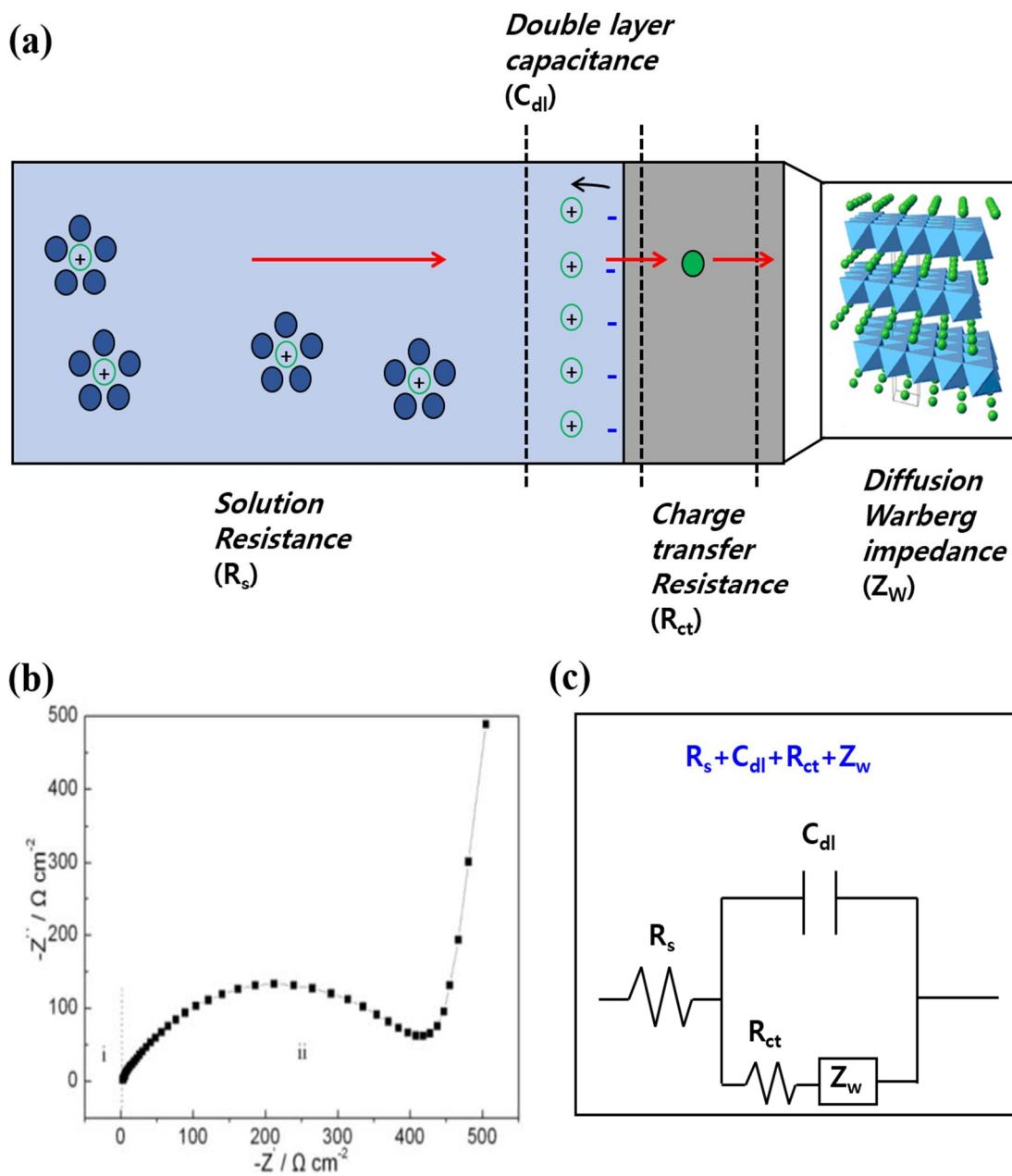
Figure 2.2. (a) The Li$^+$ diffusion mechanism of lithium ion batteries, (b) Nyquist plot of an electrode, and (c) equivalent circuit from the Nyquist plot.

2-2-2. Cyclic voltammetry (CV)

Cyclic voltammetry is typical technique that the current flow can be measured by controlling the potential of the working electrode. This method is a principle of observing the change of current while applying voltage at a constant scan rate (mV/s). This electrochemical analysis provides a lot of information, such as the oxidation and reduction mechanism of a material, the reversibility from the voltage gap of oxidation and reduction, and the reactivity from area of current x voltage [4-6]. The measurement can also calculate the diffusion coefficient of lithium ions diffused into an active material through a current change that varies with the scan rate [7, 8].

When the cyclic voltammetry applied to solid electrolyte, its purpose is to evaluate the electrochemical stability of solid electrolyte [9, 10]. The configuration of the cell for the cyclic voltammetry is mainly composed by symmetric Li/electrolyte/SUS or Cu (reference/working/counter electrodes) [9]. The stability of the solid electrolyte is evaluated by comparing the current change while the voltage is being scanned at a constant rate. This method is not an accurate for comparing the degree of reaction of the solid electrolytes, but is good at observing the reaction voltage of the electrolytes.

2-2-3. Direct current cycling (DC-cycling)

DC-cycling measurement is one of the galvanostatic measurements such as galvanostatic charge-discharge and galvanostatic intermittent titration technique. The simple electrochemical analysis is conducted by applying the constant current to a cell during charge and discharge with time cut off condition. Recently, this measurement has been used to evaluate the electrochemical stability of solid electrolyte materials (versus Li metal Li/SE/Li) [10]. Compare with cyclic voltammetry, DC-cycling is good for comparing electrochemical reactivity as well as resistance of solid electrolytes. The example of DC-cycling is shown in figure 1.12 [10]. When the solid electrolyte reacts with lithium metal, the voltage of the battery changes in the direction of increasing. The reason of increasing voltage is the resistance by SEI formation. As followed the simple ohm`s law (V=IR), the voltage increases by some resistance factor when the constant current (mA/cm^2) is applied. Because other conditions are same, the resistance is considered by SEI formation between solid electrolyte and Li metal like Li/SEI/SE. Conversely, when the voltage is maintained at a constant value,

the solid electrolyte material is considered stable with Li metal. The electrolyte may not react with Li metal or form the SEI with very slow rate. In other cases, the solid electrolyte reacts with Li metal at initial cycles and formed stable SEI. Therefore, the voltage changes do not occur after the first few cycles. This analysis is simple but gives a lot of information about electrochemical stability of a material.

2-2-4. Galvanostatic charge-discharge measurements (CD)

During galvanostatic cycling of batteries, the charge and discharge current are often expressed as a C-rate which is a measure of the rate. A C-rate of 1 C means that the necessary current is applied or drained from the battery to completely charge or discharge it in 1 hour. Since the capacity is expressed in ampere per hour, calculating the current necessary to charge or discharge a battery is straightforward.

Reference

[1] Pope, Christopher G. "X-ray diffraction and the Bragg equation." *Journal of chemical education* 74, no. 1 (1997).

[2] Hammond, Christopher, and Christopher Hammond. "The basics of crystallography and diffraction." Vol. 214. Oxford, (2001).

[3] Sheng, Lee Hwang. "Nanostructured Phosphate-based Electrode Materials for Lithium Batteries." PhD diss., (2012).

[4] Gosser, David K. "Cyclic voltammetry: simulation and analysis of reaction mechanisms." Vol. 43. New York: VCH, (1993).

[5] Kounaves, Samuel P. "Voltammetric techniques." *Handbook of instrumental techniques for analytical chemistry* (1997).

[6] Sheng, Lee Hwang. "Nanostructured Phosphate-based Electrode Materials for Lithium Batteries." PhD diss., (2012).

[7] Tang, S. B., M. O. Lai, and L. Lu. "Li-ion diffusion in highly (0 0 3) oriented $LiCoO_2$ thin film cathode prepared by pulsed laser deposition." *Journal of Alloys and Compounds* 449, no. 1-2 (2008).

[8] Wen, C. John, B. A. Boukamp, Robert A. Huggins, and W. Weppner. "Thermodynamic and mass transport properties of LiAl." *Journal of the Electrochemical Society* 126, no. 12 (1979).

[9] Neudecker, B. J., and W. Weppner. "Li_9SiAlO_8: A lithium ion electrolyte for voltages above 5.4 V." *Journal of the electrochemical society* 143, no. 7 (1996).

[10] Hood, Zachary D., Hui Wang, Amaresh Samuthira Pandian, Jong Kahk Keum, and Chengdu Liang. "Li_2OHCl crystalline electrolyte for stable metallic lithium anodes." *Journal of the American Chemical Society* 138, no. 6 (2016).

Chapter 3. Synthesis and electrochemical performance of $(100-x)(2.5Li_2S-0.5P_2S_5-LiCl)-xLiNbO_3$ (x= 0, 2, 3, 4, and 5) solid electrolyte for all-solid-state lithium batteries

3-1. Introduction

Recently, lithium-ion batteries (LIBs) have a wide range of uses, from portable electronics to electric vehicles and energy storage devices. However, there are safety issues such as explosion and ignition due to the organic liquid electrolyte of LIBs which has flammable and volatile feature [1]. To solve this problem and enhance the energy density, all-solid-state lithium batteries (ASSLBs) comprising the solid electrolyte (SE) composed of an inorganic ceramic material and polymer-based electrolytes are attracting attention. In particular, sulfide-based inorganic ceramics have high ionic conductivity and exhibit mechanically softer properties than other oxide or halide SEs which is good for making intimate contact between solid particles [2, 3].

Although the sulfide-based solid electrolytes have good properties, numerous research and developments are needed to apply and to commercialize in ASSLBs. For this reason, many attempts have been made to dope/mix various materials into the sulfide-based solid electrolyte and to optimize the synthesis process. Typically, Li-argyrodites, one of the representative sulfide electrolytes, achieved high ionic conductivity comparable to that of conventional organic liquid electrolytes through the process of doping. For example, the chlorine-rich argyrodite $Li_{5.5}PS_{4.5}Cl_{1.5}$ exhibited high ionic conductivity of 9.4 mS/cm with activation energy of 0.29eV at 25℃. And the substitution series $Li_{6-x}PS_{5-x}ClBr_x$ ($0 \leq x \leq 0.8$) has been achieved a very high conductivity of 24 mS/cm at room temperature for the composition of $Li_{5.3}PS_{4.3}ClBr_{0.7}$ [4, 5]. However, these highly conductive sulfide solid electrolytes have showed poor electrochemical stability due the electrode/electrolyte interface problem [6].

In particular, sulfide electrolytes are unstable when in contact with oxide cathodes, because it forms a space-charge layer due to the incompatibility of chemical potentials, and mutual diffusion of the S, P ions in the sulfides and transition metal ions in the cathode, leading to large interfacial resistance. Moreover, sulfide electrolytes are oxidized in the high voltage range during charging process due to their narrow electrochemical stability window, which decomposes intensively at cathode/sulfide electrolyte interface because the cathode material can provide electrons causing oxidation of sulfides. Due to the above reactions, undesirable interfacial layer forms at cathode/sulfide electrolyte interface, which hinders lithium ion migration kinetics at the interface and reduces the electrochemical performance of ASSLBs during cycling [7-10].

To solve this problem, surface modification has been used on the surface of cathodes because suitable intermediate materials are needed between the sulfide electrolyte and cathode materials to suppress the interfacial side reactions [11]. Several oxides such as $LiNbO_3$, Li_2ZrO_3 and $LiTaO_3$ were successfully applied as coating material of cathodes for ASSBs. In particular, $LiNbO_3$ has been considered as the most representative coating material because of their good ionic conductivity (10^{-5} - 10^{-6} S·cm^{-1}) and good chemical stability with sulfide electrolytes [12, 13]. However, the $LiNbO_3$ coating process for ASSBs is very expensive, because it uses mostly lithium ethoxide and niobium ethoxide with very high price as source materials to obtain a thin and uniform coating layer [14].

Therefore, instead of coating for surface of the cathode active material, we have performed an approach to increase the stability of sulfide solid electrolyte through mixing/doping to suppress interfacial resistance.

3-2. Experimental

3-2-1. Synthesis of $LiNbO_3$ nanoparticles

Firstly, $LiNbO_3$ nanoparticle was prepared by a sol-gel technique [15]. The reagent-grade $NbCl_5$ (99.99%, Sigma-Aldrich), $Li(CH_3COO)·2H_2O$ (BioXtra, Sigma-Aldrich) and citric acid (99%, Daejung chemical) were purchased and used as the starting materials. Briefly, 1.845 g of $NbCl_5$ was dissolved in 100 mL of 35% H_2O_2 and stirred in a sealed glass bottle. During the stirring process, 0.6901 g of $Li(CH_3COO)·2H_2O$ and 3.918 g of citric acid were

added slowly and then the solution was stirred at 65℃ until get a white-yellow gel. After evaporating all of the solvent, the material was dried in a vacuum oven at 120℃ for 12 hours and sintered in a furnace at 600℃ for 5 h at 5℃ min^{-1} to obtain the LiNbO$_3$ nanoparticles.

3-2-2. Preparation of LiNbO$_3$ mixed/doped Li$_6$PS$_5$Cl solid electrolyte

The LiNbO$_3$ mixed/doped Li$_6$PS$_5$Cl solid electrolyte was prepared via a high energy mechanical ball-milling and subsequent annealing process was carried out in argon filled glove box. Briefly, Li$_2$S (99.98%, Sigma-Aldrich), P$_2$S$_5$ (99%, Sigma-Aldrich), LiCl (BioXtra, ≥99.0%, Sigma-Aldrich), and the LiNbO$_3$ were weighed at the molar ratio of 98(2.5Li$_2$S:0.5P$_2$S$_5$:1LiCl)-2(LiNbO$_3$) and grinded in a mortar and pestle, and the mixture was transferred to a zirconia jar (volume: 80 mL) with 25 zirconia balls (diameter: 10 mm). Then the ball mill jar was sealed and brought out from the glove box. The solid-state reaction was conducted at 400 rpm for 15 h at room temperature using the planetary ball-milling machine. After ball milling process, the ball mill jar was bringing back to the glove box; and the product was ground for 30 minutes using mortar and pestle. The ground powder is made into pellets by applying a pressure of 30 MPa and sintered at 550℃ for 10 h with the heat rate of 2℃ min^{-1}. Finally, the pellet was crushed into powder using mortar and pestle. The obtained product was name as 98LPSCl-2LNO and the same procedure was used to prepare 97LPSCl-3LNO, 96LPSCl-4LNO and 95LPSCl-5LNO solid electrolytes. For comparison, we also prepared the LPSCl (Li$_6$PS$_5$Cl) argyrodite solid electrolyte without LNO (LiNbO$_3$) particles.

3-2-3. Characterization and electrochemical measurements

Powder X-ray Diffraction (XRD) analysis was carried out in the 2θ range of 10 to 60° using an X-ray diffractometer (Rigaku Ultima 4) with Cu-Kα radiation (λ = 1.5418 Å). Before the XRD measurement, the solid electrolytes were sealed in an airtight holder inside an Ar-filled glove box to prevent from of air and moisture. The surface morphology of samples was studied by using field-emission scanning electron microscopy (JSM-7610F, JEOL) with energy dispersive spectroscopy (x-MaxN, Oxford instruments). Laser-Raman

spectroscopic analysis was performed using a confocal Raman spectroscopic system (SR-303I-A, Andor Technology) with an excitation wavelength of 532 nm. Ionic conductivity of the electrolyte was measured by electrochemical impedance spectroscopy (EIS) in the frequency range of 7 MHz to 1 Hz with an applied an amplitude of 50 mV using Biologic (SP-300). For this measurement, the solid electrolyte powder (~ 250 mg) was pelletized in an In/SE/In symmetric cell with 10 mm diameter under a pressure of 30 MPa.

To evaluate the electrochemical stability window of the solid electrolyte, cyclic voltammetry was carried out between -0.5 V and 5 V (vs. Li) at a scan rate of 1 mV s^{-1} on SUS(stainless steel)/SE/Li cells using a potentiostat/galvanostatic system (SP-300, BioLogic). DC cycling was conducted on Li/SE/Li at a constant current density of 0.5 mA cm^{-2} for 100 h using a battery tester (Maccor, Korea Thermo-tech Co. Ltd) to analyze the compatibility of the solid electrolyte toward Li metal.

The galvanostatic charge – discharge performance of ASSLBs with as-synthesized solid electrolytes was conducted. Before the charge–discharge measurements, the composite cathode for ASSLBs was prepared by mixing the bare (uncoated) NCM-811 active material, solid electrolyte, and conductive material (Super-P) with a weight ratio of 60:36:4 by hand grinding. For the fabrication of 2032-type all-solid-state cells, the solid electrolyte (200 mg) was put into a 16 mm-diameter mold and compressed by applying a pressure of 30 MPa. After that, as-prepared composite cathode powder (20 mg) was placed on one side of the solid electrolyte layer and a CNT current collector was attached thereon, and then pressed under 30 MPa. Finally, 50 mg of the Li-In alloy (Li: In = 0.5:1) was sprinkled on the other side of SE layer as an anode and a copper current collector was loaded on top of the anode, and then pressed together at 30 MPa pressure. All above the fabrication procedures were conducted in an Ar-filled glove box. The galvanostatic charge-discharge measurement for the ASSLBs was performed on a battery cycling system (WBCS3000S, WonAtech) at 25℃. The voltage range was 1.9 V to 3.7 V (vs. Li-In) at different current densities from 0.05 C (17 mA g^{-1}) to 0.3 C (102 mA g^{-1}). The EIS measurements of the fabricated ASSLBs for before/after charge-discharge were measured with the frequency range of 7 MHz to 1 Hz/0.01 Hz by using a SP-300 analyzer (Biologic).

3-3. Results and discussion

3-3-1. Structural analysis of $LiNbO_3$ mixed Li_6PS_5Cl solid electrolyte

The X-ray diffraction (XRD) and Raman spectra were used to identify crystalline phases and components of the solid electrolytes. The XRD patterns of the synthesized (100-x)(LPSCl)-xLNO ($0 \leq x \leq 5$) solid electrolytes are shown in Figure 3.1. All the solid electrolytes are exhibiting argyrodite-like crystalline phase of Li_7PS_6 (JCPDS-34-0688) in cubic phase with a space group F$\overline{4}$3m [16, 17]. The main diffraction peaks at $2\theta = 15.4°$, 17.8°, 25.4°, 29.8°, 31.2°, 39.7°, 44.9°, 47.7° and 52.3° can be indexed to (111), (200), (220), (311), (222), (331), (422), (511) and (440) planes, respectively. The argyrodite phase of Li_6PS_5Cl crystal structure was maintained despite the incorporation of $LiNbO_3$. While adding small amount of $LiNbO_3$ (x = 2), we observed only argyrodite-type peaks and no impurity peaks were detected. Further increasing the concentration of $LiNbO_3$ (x $\geq$ 3), minor by-product phase corresponding to $LiNbS_2$ were observed at $2\theta = 13.4°$, 33.6° and 41.6° attributing to (0 0 0 2), (1 0 -1 2), and (1 0 -1 4) planes in hexagonal crystal system with a space group P6$_3$/mmc. Besides, the impurity peaks appear at $2\theta = 34.5°$ and 49.8° when x $\geq$ 4, which were can be corresponds to LiCl. The relative intensity of the $LiNbS_2$ peaks decreases and the impurity peaks corresponding to LiCl increases with the further of the $LiNbO_3$ doping amount (x = 5), suggesting that there is a limited solubility of Nb and O substitution. In deep understanding, we believed the following hypothesis. At low $LiNbO_3$ concentration (x = 2), it cannot be observed that any by-product or residual precursor phase, but only the peak shift to lower angle was observed in XRD patterns. This indicates that the doped material ($LiNbO_3$) may intercalate within the argyrodite crystal and increased its volume [18]. Further increasing the $LiNbO_3$ concentration (x $\geq$ 3) to sample, the peaks showed a shift along with $LiNbS_2$ by-product. This indicates that the partial amount of $LiNbO_3$ is intercalated within the argyrodite crystal, and the remaining part of $LiNbO_3$ may involve in reaction with excess sulfur or P_2S_5 to produce $LiNbS_2$. For the higher $LiNbO_3$ content (x = 5), we observed not only the peak shift toward lower angle but also the higher peak intensity of the LiCl impurities than that of the $LiNbS_2$ by-product. This indicates that the small amount of $LiNbO_3$ may involve in reaction with excess sulfur or P_2S_5 and produce $LiNbS_2$. Compared to the x = 3 and 4 samples, most of P_2S_5 would be involved in the reaction due to excess $LiNbO_3$, which could create a chemical imbalance and promote the formation of LiCl impurities. It has been

reported that a phenomenon similar to this result commonly occurred in metal oxide doped/mixed argyrodite [19, 20].
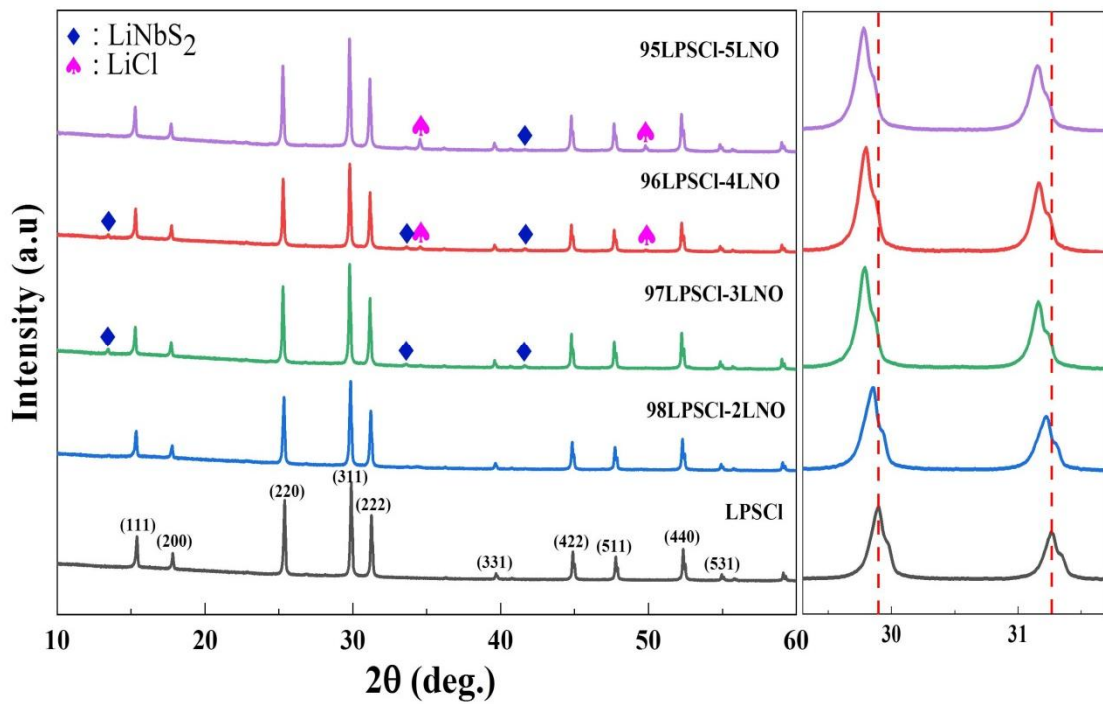

Figure 3.1. Powder X-ray diffraction patterns of $(100-x)(2.5Li_2S-0.5P_2S_5-LiCl)$-$xLiNbO_3$ $(0 \leq x \leq 5)$ solid electrolytes.

The influence of Nb and O doping on the structural characteristic of the solid electrolyte was analyzed by laser Raman spectroscopy. Figure 3.2 shows the laser Raman spectra of prepared solid electrolytes in the frequency range of 300-600 cm^{-1}. We have observed the characteristic peaks at 421, 571, and 594 cm^{-1} are attributed to the PS_4^{3-} tetrahedral group [21]. The strongest peak at 421 cm^{-1}, corresponding to the symmetric stretching vibration mode of the P-S bond in the PS_4^{3-}, keeps unchanged position with increasing of $LiNbO_3$ concentration. Although the peak intensity decreases with increasing of $LiNbO_3$ in the doped systems, there is no peak split or shift. This result indicates that the incorporation of $LiNbO_3$ in the argyrodite system has a non-destructive effect on the local structure of PS_4^{3-} unit and does not change the P-S bonds. Therefore, it is believed that the basic framework of the synthesized solid electrolytes is maintained with LPSCl argyrodite system.
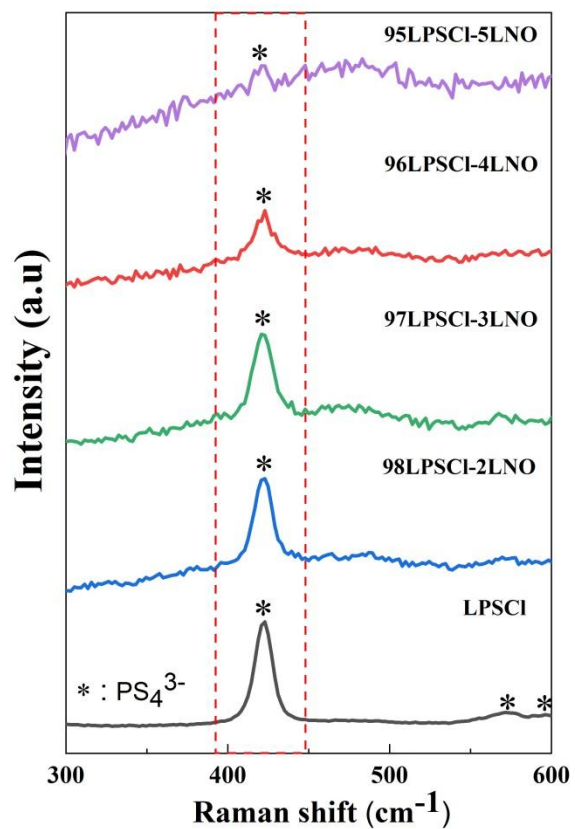
Figure 3.2. Laser Raman spectra of $(100-x)(2.5Li_2S-0.5P_2S_5-LiCl)-xLiNbO_3$ ($0 \leq x \leq 5$) solid electrolytes.

Figure 3.3 shows the SEM images of all as-prepared samples. The morphology of the Nb and O co-doped electrolytes is similar to that of the pristine sample, Li_6PS_5Cl. All of the solid electrolytes consist of irregular particles which are size ranges from one to several micrometers. The $LiNbO_3$-free LPSCl displays that round-shaped small particles clustered together, whereas the $LiNbO_3$-doped LPSCl consists of relatively large particles are packed together. The EDS mapping of the (100-x)(LPSCl)-xLNO (x = 2, 3, 4, and 5) demonstrates the elements of P, S, Cl, O and Nb. It is observed that the Nb wt% content in EDS mapping increased with increasing Nb doping amount in solid electrolyte, and all elements are distributed uniformly without segregation or aggregation, suggesting that successful doping/mixing of Nb and O on Li_6PS_5Cl.

Figure 3.3. FE-SEM images of (a, b) LPSCl, (c, d) 98LPSCl-2LNO, (e, f) 97LPSCl-3LNO, (g, h) 96LPSCl-4LNO and (i, j) 95LPSCl-5LNO solid electrolytes.

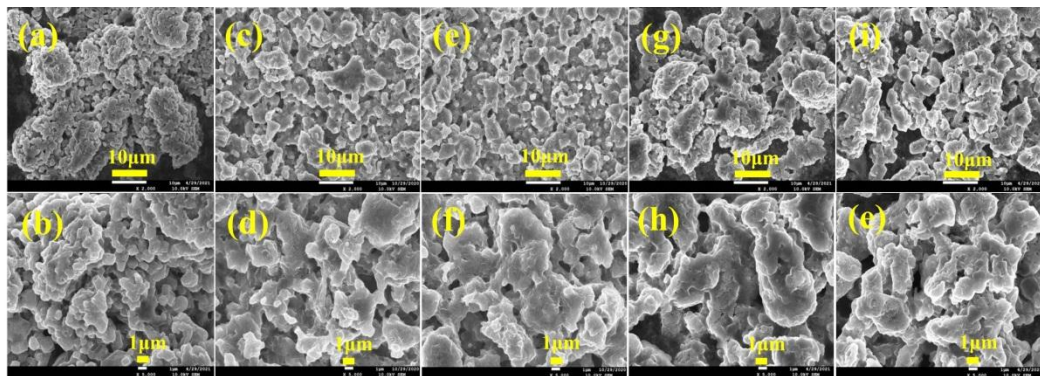3.2 Electrochemical performance

Electrochemical impedance spectroscopy (EIS) analysis was performed for the all-prepared solid electrolytes at room temperature. The ionic conductivity of the solid electrolytes was calculated from EIS analysis and the corresponding Nyquist spectra are shown in Figure 3.4. The obtained Nyquist spectra were fitted with equivalent circuit with the component of R(CR)(CR)W using ZSimpwin software. However, the impedance plots did not show clear semicircles corresponding to contribution from the bulk and grain boundary resistance, thus the component separation for resistance could not be achieved. Therefore, the resistance of the fitting value which is consistent with the intercept of the horizontal axis in the EIS curve was considered as the total resistance. The calculated ionic conductivity of $(100-x)(LPSCl)-xLNO$ ($0 \leq x \leq 5$) varied slightly with the concentration of $LiNbO_3$ as listed in Table 3.1. It is observed that the conductivity increases with increasing the doping amount from LNO from $x = 1$ to 4. The prepared 96LPSCl-4LNO solid electrolyte exhibited the highest ionic conductivity value of 4.29×10^{-3} S cm^{-1} at room temperature, and higher than LPSCl (3.23×10^{-3} S cm^{-1}) solid electrolyte. The substitution of Nb on LPSCl argyrodite system could offset the negative effect of O doping on ionic conductivity. And Nb could also partially incorporate on argyrodite structure and introduce more Li defects or vacancies which could contribute to the Li ion conductivity [22]. However, further increasing the LNO concentration, the ionic conductivity suddenly diminished to 2.84×10^{-3} S cm^{-1} (95LPSCl-5LNO), suggesting that the limitation solubility of the Nb incorporation in the lattice. In addition, the gradually increased LiCl impurity phases, as can be observed from the XRD patterns, could lead to decrease the ionic conductivity of the solid electrolyte. Although the $LiNbS_2$ by-product appears for electrolyte samples when $x \geq 3$, 96LPSCl-4LiNbO$_3$ solid electrolyte has relatively weak intensity of the LiCl impurity peak and high ionic conductivity over the entire composition range. Therefore, it was expected to benefit a good battery performance.
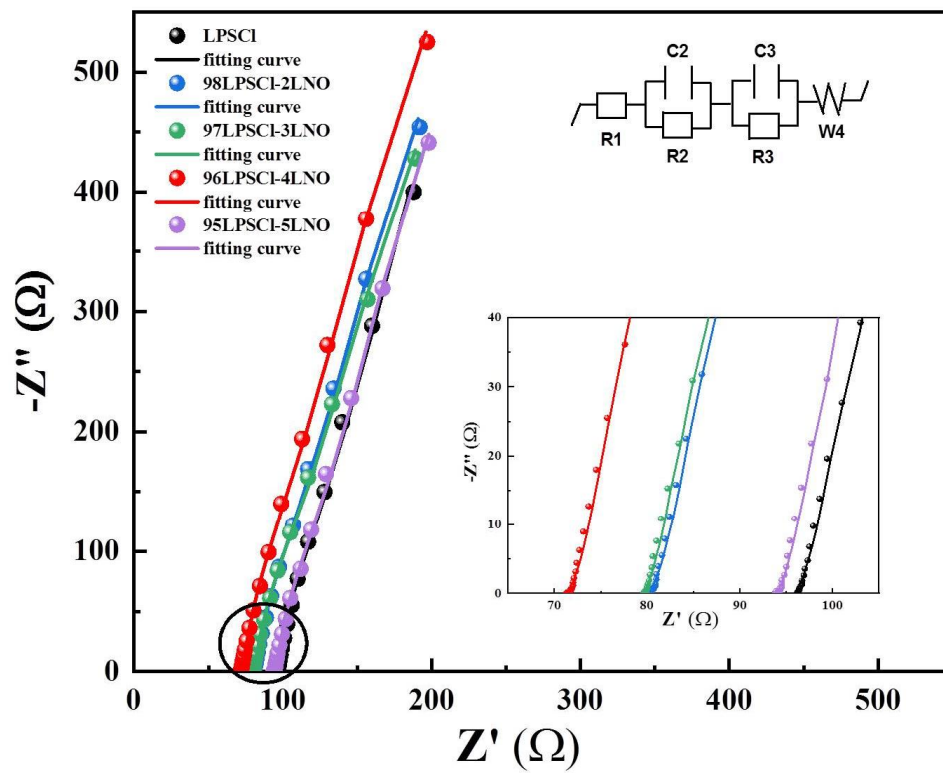
Figure 3.4. Nyquist plots of (100-x)(2.5Li$_2$S-0.5P$_2$S$_5$-LiCl)-xLiNbO$_3$ (0 ≤ x ≤ 5) solid electrolytes at room temperature.

Table 3.1. The ionic conductivity of the (100-x)(2.5Li_2S-0.5P_2S_5-LiCl)-xLiNbO$_3$

(x= 0, 2, 3, 4, and 5) at RT.

Solid electrolyte	Resistance (Ω)	Ionic conductivity (S cm^{-1})
Li$_6$PS$_5$Cl (x = 0)	95.75	3.23 x 10^{-3}
98LPSCl-2LNO (x = 2)	79.97	3.68 x 10^{-3}
97LPSCl-3LNO (x = 3)	79.33	3.69 x 10^{-3}
96LPSCl-4LNO (x = 4)	71.16	4.29 x 10^{-3}
95LPSCl-5LNO (x = 5)	100.9	2.84 x 10^{-3}

Electrochemical stability analysis of the solid electrolytes was performed by cyclic voltammetry. The CV graphs of the stainless steel/ (100-x)(LPSCl)-xLNO (x = 0 and 4) /Li cell are shown in Figure 3.5a and 3.5b. It can be seen that the electrochemical behavior is almost identical to each other. During the scanning cycle, no other reduction or oxidation peaks were observed except the lithium deposition ($Li^+ + e^- \rightarrow Li$) and dissolution ($Li \rightarrow Li^+ + e^-$) peaks between -0.5 V and 0.5 V. And both solid electrolyte samples exhibit wide electrochemical window up to 5 V (vs Li/Li^+). Similarly, as shown in Figure 5c and 5d, DC stability test profiles of LPSCl and 96LPSCl-4LNO solid electrolyte display a stable behavior with metallic lithium even after 100 charge-discharge cycles, indicating that both of electrolytes are compatible with the lithium anode.
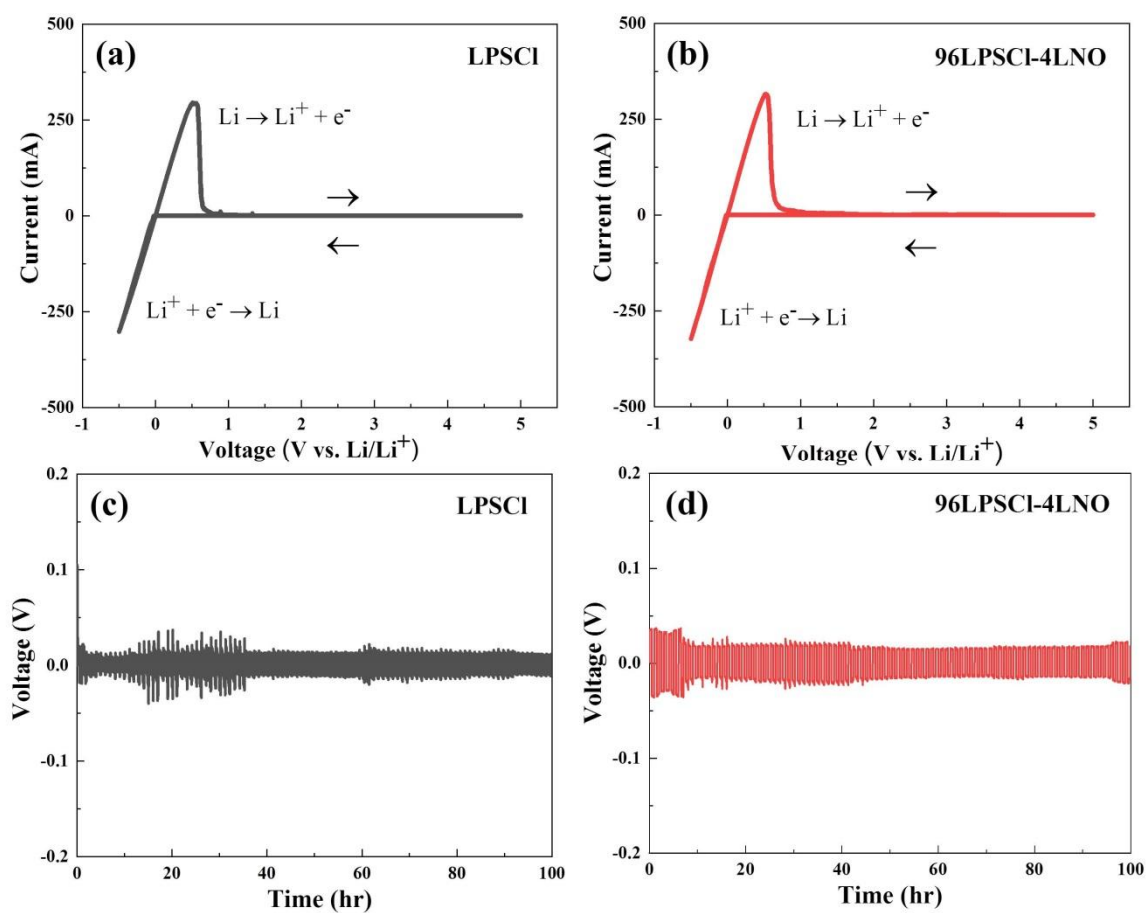
Figure 3.5. (a)&(b) Cyclic voltammogram and (c)&(d) DC stability curve of LPSCl and

96LPSCl-4LNO solid electrolytes measured at room temperature.

To investigate the electrochemical performance of the solid electrolyte samples, ASSLBs were fabricated with composite cathode and Li-In used anode material, respectively. The composite cathode for ASSLBs was mixture of cathode active material (NCM-811), conductive material (Super-P) and solid electrolyte. Here, we believed that the addition of $LiNbO_3$ may stabilize the interfacial stability between the cathode active material and solid electrolyte during the charge–discharge process. For better understanding the effect of LNO doping/mixing towards the electrochemical performance, we have prepared three types of cells having the different composite-cathode and solid electrolyte, as shown in Table 2. Cell 1 was prepared using pristine NCM-811 and LPSCl without $LiNbO_3$ mixing/doping. Cell 2 was composed of pristine NCM-811 cathode and 96LPSCl-4LNO. Cell 1 and Cell 2 used same solid electrolyte for composite-cathode and electrolyte layer between the cathode and anode. In contrast, Cell 3 consisted of composite-cathode containing pristine NCM-811 and 96LPSCl-4LNO and electrolyte layer prepared using LPSCl without $LiNbO_3$ mixing/doping, i.e., the solid electrolyte for composite-cathode and electrolyte layer was different.

Figure 3.6a shows the initial charge-discharge curves of the ASSLBs based on Li_6PS_5Cl and 96LPSCl-4LNO solid electrolytes at 0.05C-rate in the voltage range of 1.9-3.7 V. The first discharge capacity and Coulombic efficiency of the three cells are summarized in Table 3.2. The first charge and discharge specific capacity of Cell 1 is 215.2 and 163.4 mAh g^{-1}, with Coulombic efficiency of 75.9 %. In contrast, Cell 2 achieves a high initial charge and discharge capacity of 246.6 and 188.7 mAh g^{-1} with Coulombic efficiency of 76.5 %, suggesting that 4 mol % $LiNbO_3$ doping/mixing in LPSCl solid electrolyte contributes to improve performance for ASSLBs. However, the difference between the two electrolyte samples in ionic conductivity was not significant. The ionic conductivity of 96LPSCl-4LNO (4.29 mS cm^{-1}) evaluated in the previous section is only 1.3 times higher than that of LPSCl (3.23 mS cm^{-1}). To reduce the effect of increased conductivity and investigate the enhanced interfacial stability by $LiNbO_3$ mixing/doping, Cell 3 used LPSCl as solid electrolyte layer, and just used 96LPSCl-4LNO electrolyte for composite cathode. Although, higher conductivity of 96LPSCl-4LNO electrolyte still affect the ionic movement in the composite cathode, interfacial stabilization effect by $LiNbO_3$ mixing/doping could more influence on the electrochemical performance of the cell. As shown in Figure 3.6a and Table 3.2, the cell 3 demonstrates that the initial charge and discharge specific capacity of 236.0 and 179.9 mAh

g^{-1} with Coulombic efficiency of 76.2 %. Comparing the discharge capacities, Cell 2 delivers 8.8 mAh g^{-1} higher capacity than Cell 3, which may induced by 96LPSCl-4LNO having higher ionic conductivity than LPSCl in a solid electrolyte layer. However, the difference in discharge capacity between Cell 3 and Cell 1 is somewhat large (~16.5 mAh g^{-1}). As a result of this obvious difference indicates that 96LPSCl-4LNO solid electrolyte in the composite cathode not only has a relatively high ionic conductivity but also stabilizes the interface with the cathode active material (NCM-811).
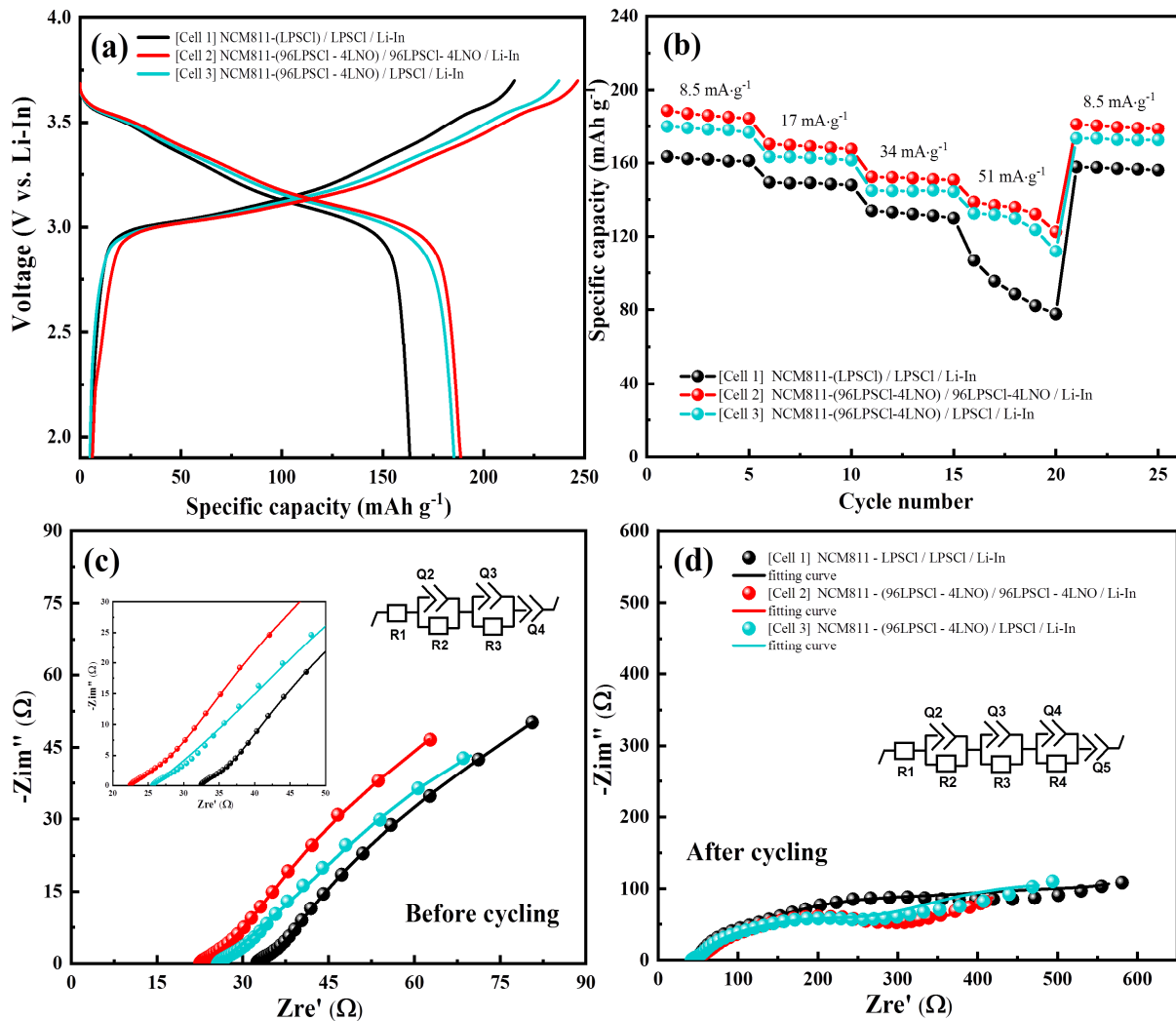
Figure 3.6. (a) Initial charge–discharge curves and (b) rate performance of the NCM-(SE)/SE/Li-In ASSLBs at 25℃. (c) Impedance spectra of the NCM-(SE)/SE/Li-In ASSLBs before and after cycling.

Table 3.2. The discharge capacity and Coulombic efficiency of ASSLBs with (100-x)(2.5Li$_2$S-0.5P$_2$S$_5$-LiCl)-xLiNbO$_3$ (x = 0 and 4) at 0.05C-rate.

Cell name	Solid electrolyte	Solid electrolyte for composite cathode	1st Discharge capacity (mAh g^{-1})	1st Coulombic efficiency (%)
Cell 1	Li$_6$PS$_5$Cl	Li$_6$PS$_5$Cl	163.4	75.9
Cell 2	96LPSCl-4LNO	96LPSCl-4LNO	188.7	76.5
Cell 3	Li$_6$PS$_5$Cl	96LPSCl-4LNO	179.9	76.2

Additionally, Figure 3.6b compares the cycling performance at different current densities for three cells. All of the cells exhibit an excellent cycling stability and close to 100% Coulombic efficiency, except for the step of 0.3 C-rate. Among the assembled solid-state batteries, Cell 2 demonstrates good capacity retention and the highest specific capacity in all stages with different C-rates, confirming that use of 96LPSCl-4LNO solid electrolyte could effectively improve the battery performance. Moreover, it can be seen that the rate performance of Cell 3 also significantly enhanced than Cell 1, indicating that the 96LPSCl-4LNO electrolyte which was included in composite cathode decrease the interfacial resistance for cathode active material and provide stable interfacial contact between cathode electrode and solid electrolyte.

The EIS spectra of three NCM-(SE)/SE/Li-In ASSLBs before/after charge − discharge cycle tests were recorded between the frequency ranges from 7 MHz to 1 Hz/0.01 Hz as shown in Figure 3.6c and 3.6d. In order to clearly distinguish the resistance, the equivalent circuits were used for fitting the ASSLBs. In Nyquist plot from the EIS spectra, the intercept of the horizontal axis in the high frequency region is attributed to the internal resistance (R1) of the solid electrolyte. The resistance from the semicircle on the horizontal axis at the middle frequency region represents the charge transfer resistance (R2) and the interfacial resistance (R3) between the cathode electrode and solid electrolyte. Furthermore, the resistance (R4) at the low frequency region came from the Li-In anode electrode side. As demonstrated in Table 3.3, the internal resistances (R1) of the batteries assembled with LPSCl/LPSCl (Cell 1) and 96LPSCl-4LNO/96LPSCl-4LNO (Cell 2) (SE/ SE of composite cathode) before cycling are

32.32 Ω and 22.22 Ω, respectively. Similar to the trend of the ionic conductivity values of the solid electrolyte measured above, although the internal resistance from the solid electrolyte of the cell with 96LPSCl-4LNO/96LPSCl-4LNO is smaller than that of the LPSCl/LPSCl cell, no significant difference is observed. In addition, compared to the battery integrated with LPSCl/LPSCl (SE/ SE of composite cathode), which interfacial resistance (R3) increases from 55.28 Ω to 301.9 Ω after cycling, for the ASSLB with 96LPSCl-4LNO/96LPSCl-4LNO, the interfaced resistance (R3) increases from 30.86 Ω to 259.6 Ω. It suggests that $LiNbO_3$ mixing/doping into the LPSCl argyrodite system could improve not only the reaction kinetics for ASSLBs but also the interfacial stability between cathode electrode and solid electrolyte. To explore the effect of the 96LPSCl-4LNO solid electrolyte of the composite cathode, the impedance properties of the Cell 3 were also examined. The interface impedance (R3) of Cell 3 after cycling is 250.2 Ω, which is lower than that of Cell 1 (301.9 Ω). It is confirmed that while the interfacial resistance between the bare NCM811 with 96LPSCl-4LNO electrolyte of composite cathode and the LPSCl solid electrolyte increase as well during cycling, the changes are small compared to the bare NCM811 cathode material in contact with the LPSCl solid electrolyte. This result suggests that the 96LPSCl-4LNO solid electrolyte of the composite cathode reduces the interfacial resistance between cathode active material and solid electrolyte during the cycling processes, which is consistent with the result of the discharge capacity profiles.

Table 3.3 Impedance fitting data from the NCM-(SE)/ SE /Li-In ASSLBs before and after cycling

Cell name	Calculated impedance value of fabricated ASSLBs								
	Before Cycling				After Cycling				
	R_1	R_2	R_3	R_{total}	R_1	R_2	R_3	R_4	R_{total}
Cell 1	32.32	3.63	55.28	91.23	43.25	17.82	301.9	332.1	695.07
Cell 2	22.22	8.317	30.86	61.4	40.66	37.55	259.6	4.839	342.65
Cell 3	25.66	8.876	42.41	76.964	41.05	6.1	250.2	348.5	645.85

3.3 Interfacial analysis

To investigate the effect of the 96LPSCl-4LNO solid electrolyte on the interface with cathode active material in composite cathode of ASSLBs, the EDS mapping analysis was conducted and the corresponding images are shown in Figure 3.7. As depicted in Figure 3.7, the Nb content was confirmed by EDS mapping of the NCM811 of the Cell 2, and it could be inferred that Nb in the 96LPSCl-4LNO electrolyte of the composite cathode could act as a coating layer by covering the NCM particles and improve the interfacial stability between the cathode material and solid electrolyte during the cycling.
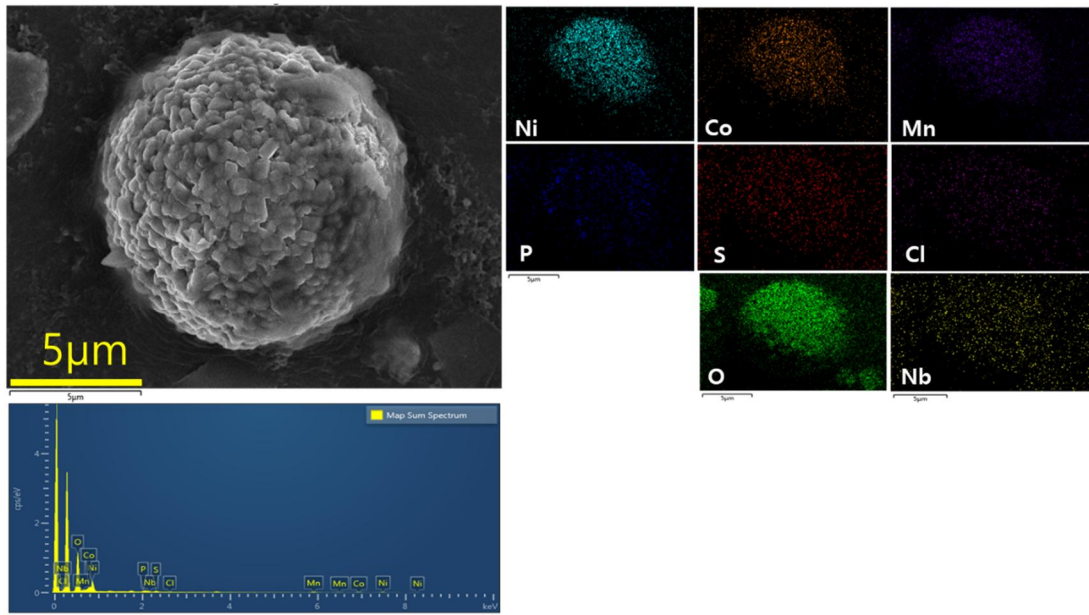
Figure 3.7 FE-SEM and EDS mapping images of 96LPSCl-4LNO solid

electrolyte/NCM811 composite cathode after charge-discharge cycles

3.4 Conclusions

LiNbO$_3$ coating materials mixed/doped Li$_6$PS$_5$Cl solid electrolyte was prepared by high energy ball mill method for improving the electrochemical performance of ASSLBs. The addition of LiNbO$_3$ to Li$_6$PS$_5$Cl solid electrolyte is not only enhanced the ionic conductivity but also created the intermediate layer between the electrolyte and electrode. The addition of LiNbO$_3$ to Li$_6$PS$_5$Cl solid electrolyte was confirmed by XRD and laser Raman spectroscopy analysis. EIS analysis was used to calculate the ionic conductivity of the prepared solid electrolytes and the 96LPSCl-4LNO solid electrolyte exhibited the highest ionic conductivity of 4.29 mS cm^{-1} at room temperature compared to other solid electrolytes. The electrochemical stability of the solid electrolyte against lithium metal was studied by cyclic voltammetry and DC polarization techniques. Furthermore, the ASSLBs with the prepared LiNbO$_3$ mixed/doped Li$_6$PS$_5$Cl solid electrolyte (96LPSCl-4LNO)/NCM811 composite cathode achieved higher specific capacity (188.7 mAh g^{-1}) and the C-rate performance than ASSLBs based on the Li$_6$PS$_5$Cl solid electrolyte/NCM811 composite cathode (163.4 mAh g^{-1}). These high specific capacity values and good cycling performance were due to the improved stability between the solid electrolyte and the cathode material during the electrochemical reaction.

References

[1] Li, X.; Guan, H.; Ma, Z.; Liang, M.; Song, D.; Zhang, H.; Shi, X.; Li, C.; Jiao, L.; Zhang, L. In/Ex-Situ Raman Spectra Combined with EIS for Observing Interface Reactions between Ni-Rich Layered Oxide Cathode and Sulfide Electrolyte. *Journal of Energy Chemistry* **2020**, *48*, 195–202. https://doi.org/10.1016/j.jechem.2020.01.021.

[2] Seino, Y.; Ota, T.; Takada, K.; Hayashi, A.; Tatsumisago, M. A Sulphide Lithium Super Ion Conductor Is Superior to Liquid Ion Conductors for Use in Rechargeable Batteries. *Energy Environ. Sci.* **2014**, *7* (2), 627–631. https://doi.org/10.1039/C3EE41655K.

[3] Kamaya, N.; Homma, K.; Yamakawa, Y.; Hirayama, M.; Kanno, R.; Yonemura, M.; Kamiyama, T.; Kato, Y.; Hama, S.; Kawamoto, K.; Mitsui, A. A Lithium Superionic Conductor. *Nature Mater* **2011**, *10* (9), 682–686. https://doi.org/10.1038/nmat3066.

[4] Adeli, P., Bazak, J. D., Huq, A., Goward, G. R., & Nazar, L. F. Influence of Aliovalent Cation Substitution and Mechanical Compression on Li-Ion Conductivity and Diffusivity in Argyrodite Solid Electrolytes. *Chemistry of Materials* **2020**, *33* (1), 146-157.doi:10.1021/acs.chemmater.0c03090.

[5] Patel, S. V., Banerjee, S., Liu, H., Wang, P., Chien, P.-H., Feng, Y.-Y. Tunable Lithium Ion Transport in Mixed-Halide Argyrodites $Li_{6-x}PS_{5-x}ClBr_x$: An Unusual Compositional Space. *Chemistry of Materials* **2021**, *33* (4), 1435–1443. doi:10.1021/acs.chemmater.0c04650.

[6] Wang, C.; Adair, K. R.; Liang, J.; Li, X.; Sun, Y.; Li, X.; Wang, J.; Sun, Q.; Zhao, F.; Lin, X.; Li, R.; Huang, H.; Zhang, L.; Yang, R.; Lu, S.; Sun, X. Solid-State Plastic

Crystal Electrolytes: Effective Protection Interlayers for Sulfide-Based All-Solid-State Lithium Metal Batteries. *Advanced Functional Materials* **2019**, *29* (26), 1900392. https://doi.org/10.1002/adfm.201900392.

[7] Zhang, J.; Zheng, C.; Li, L.; Xia, Y.; Huang, H.; Gan, Y.; Liang, C.; He, X.; Tao, X.; Zhang, W. Unraveling the Intra and Intercycle Interfacial Evolution of Li_6PS_5Cl-Based All Solid-State Lithium Batteries. *Advanced Energy Materials* **2020**, *10* (4), 1903311. https://doi.org/10.1002/aenm.201903311.

[8] Deng, S.; Li, X.; Ren, Z.; Li, W.; Luo, J.; Liang, J.; Liang, J.; Banis, M. N.; Li, M.; Zhao, Y.; Li, X.; Wang, C.; Sun, Y.; Sun, Q.; Li, R.; Hu, Y.; Huang, H.; Zhang, L.; Lu, S.; Luo, J.; Sun, X. Dual-Functional Interfaces for Highly Stable Ni-Rich Layered Cathodes in Sulfide All-Solid-State Batteries. *Energy Storage Materials* **2020**, *27*, 117–123. https://doi.org/10.1016/j.ensm.2020.01.009.

[9] Du, M.; Liao, K.; Lu, Q.; Shao, Z. Recent Advances in the Interface Engineering of Solid-State Li-Ion Batteries with Artificial Buffer Layers: Challenges, Materials, Construction, and Characterization. *Energy Environ. Sci.* **2019**, *12* (6), 1780–1804. https://doi.org/10.1039/C9EE00515C.

[10] Zhu, Y., He, X., & Mo, Y. Origin of Outstanding Stability in the Lithium Solid Electrolyte Materials: Insights from Thermodynamic Analyses Based on First Principles Calculations. ACS Applied Materials & Interfaces **2015**, *7* (42), 2368523693. doi:10.1021/acsami.5b07517.

[11] Li, X.; Sun, Q.; Wang, Z.; Song, D.; Zhang, H.; Shi, X.; Li, C.; Zhang, L.; Zhu, L. Outstanding Electrochemical Performances of the All-Solid-State Lithium Battery

Using Ni-Rich Layered Oxide Cathode and Sulfide Electrolyte. *Journal of Power Sources* **2020**, *456*, 227997. https://doi.org/10.1016/j.jpowsour.2020.227997.

[12] Nakamura, H.; Kawaguchi, T.; Masuyama, T.; Sakuda, A.; Saito, T.; Kuratani, K.; Ohsaki, S.; Watano, S. Dry Coating of Active Material Particles with Sulfide Solid Electrolytes for an All-Solid-State Lithium Battery. *Journal of Power Sources* **2020**, *448*, 227579. https://doi.org/10.1016/j.jpowsour.2019.227579.

[13] Li, X.; Liang, M.; Sheng, J.; Song, D.; Zhang, H.; Shi, X.; Zhang, L. Constructing Double Buffer Layers to Boost Electrochemical Performances of NCA Cathode for ASSLB. *Energy Storage Materials* **2019**, *18*, 100–106. https://doi.org/10.1016/j.ensm.2018.10.003.

[14] Culver, S. P., Koerver, R., Zeier, W. G., & Janek, J. On the Functionality of Coatings for Cathode Active Materials in Thiophosphate-Based All-Solid-State Batteries. *Advanced Energy Materials* **2019**, 1900626. doi:10.1002/aenm.201900626

[15] Kim, Y.-J.; Rajagopal, R.; Kang, S.; Ryu, K.-S. Novel Dry Deposition of $LiNbO_3$ or Li_2ZrO_3 on $LiNi_{0.6}Co_{0.2}Mn_{0.2}O_2$ for High Performance All-Solid-State Lithium Batteries. *Chemical Engineering Journal* **2020**, *386*, 123975. https://doi.org/10.1016/j.cej.2019.123975.

[16] Huang, W.; Cheng, L.; Hori, S.; Suzuki, K.; Yonemura, M.; Hirayama, M.; Kanno, R. Ionic Conduction Mechanism of a Lithium Superionic Argyrodite in the Li–Al–Si–S–O System. *Mater. Adv.* **2020**, *1* (3), 334–340. https://doi.org/10.1039/D0MA00115E.

[17] Patel, S. V.; Banerjee, S.; Liu, H.; Wang, P.; Chien, P.-H.; Feng, X.; Liu, J.; Ong, S. P.; Hu, Y.-Y. Tunable Lithium-Ion Transport in Mixed-Halide Argyrodites $Li_{6-x}PS_{5-x}ClBr_x$: An Unusual Compositional Space. *Chem. Mater.* **2021**, *33* (4), 1435–1443. https://doi.org/10.1021/acs.chemmater.0c04650.

[18] Zhang, J.; Li, L.; Zheng, C.; Xia, Y.; Gan, Y.; Huang, H.; Liang, C.; He, X.; Tao, X.; Zhang, W. Silicon-Doped Argyrodite Solid Electrolyte Li_6PS_5I with Improved Ionic Conductivity and Interfacial Compatibility for High-Performance All-Solid-State Lithium Batteries. *ACS Appl. Mater. Interfaces* **2020**, *12* (37), 41538–41545. https://doi.org/10.1021/acsami.0c11683.

[19] Lee, Y.; Jeong, J.; Lim, H.-D.; Kim, S.-O.; Jung, H.-G.; Chung, K. Y.; Yu, S. Superionic Si-Substituted Lithium Argyrodite Sulfide Electrolyte $Li_{6+x}Sb_{1-x}Si_xS_5I$ for All-Solid-State Batteries. *ACS Sustainable Chem. Eng.* **2021**, *9* (1), 120–128. https://doi.org/10.1021/acssuschemeng.0c05549.

[20] Song, Y. B.; Kim, D. H.; Kwak, H.; Han, D.; Kang, S.; Lee, J. H.; Bak, S.-M.; Nam, K.-W.; Lee, H.-W.; Jung, Y. S. Tailoring Solution-Processable Li Argyrodites $Li_{6+x}P_{1-X}M_xS_5I$ (M = Ge, Sn) and Their Microstructural Evolution Revealed by Cryo-TEM for All-Solid-State Batteries. *Nano Lett.* **2020**, *20* (6), 4337–4345. https://doi.org/10.1021/acs.nanolett.0c01028.

[21] Chen, T.; Zeng, D.; Zhang, L.; Yang, M.; Song, D.; Yan, X.; Yu, C. Sn-O Dual-Doped Li-Argyrodite Electrolytes with Enhanced Electrochemical Performance. *Journal of Energy Chemistry* **2021**, *59*, 530–537. https://doi.org/10.1016/j.jechem.2020.11.031.

[22] Ahmad, N.; Zhou, L.; Faheem, M.; Tufail, M. K.; Yang, L.; Chen, R.; Zhou, Y.; Yang, W. Enhanced Air Stability and High Li-Ion Conductivity of $Li_{6.988}P_{2.994}Nb_{0.2}S_{10.934}O_{0.6}$ Glass–Ceramic Electrolyte for All-Solid-State Lithium–Sulfur Batteries. *ACS Appl. Mater. Interfaces* **2020**, *12* (19), 21548–21558. https://doi.org/10.1021/acsami.0c00393.

Chapter 4. Summary

We have prepared the $LiNbO_3$ coating material mixed/doped Li_6PS_5Cl solid electrolyte for improving the ionic conductivity and the promoting the interfacial stability between the cathode active material and solid electrolyte.

First, the different molar ratios of $LiNbO_3$ mixed/doped Li_6PS_5Cl solid electrolyte were prepared by high energy ball milling and heat treatment process. Among the prepared solid electrolytes, $96(Li_6PS_5Cl)-4(LiNbO_3)$ solid electrolyte showed the highest ionic conductivity value of 4.29 mS cm^{-1} at room temperature. Moreover, the effect of the addition of $LiNbO_3$ was confirmed by charge–discharge measurement and electrochemical impedance spectroscopy (EIS). The ASSLB assembled based on the prepared $LiNbO_3$ mixed/doped Li_6PS_5Cl solid electrolyte/ bare-NCM811 composite-cathode exhibited a high specific capacity (188.69 mAh g^{-1}) and improved the electrochemical stability compared to the cell with Li_6PS_5Cl solid electrolyte/ bare NCM811 composite-cathode (163.41 mAh g^{-1}).

Therefore, we believed that the synthesized solid electrolyte enhanced the performance of the ASSLBs by improving the interfacial stability with the cathode.